Estimating C_n^2 over snow and sea ice from meteorological data

Edgar L Andreas*

NOAA/ERL Wave Propagation Laboratory, 325 Broadway, Boulder, Colorado 80303-3328

Received September 22, 1987; accepted December 7, 1987

Because turbulent fluctuations in the atmospheric refractive index (n) at a wavelength λ are related to fluctuations in the temperature (t) and the humidity (q) by $n = A(\lambda, P, T, Q)t + B(\lambda, P, T, Q)q$, it is possible to estimate the refractive-index structure parameter C_n^2 from meteorological quantities. I describe and evaluate two such estimation procedures, one based on the velocity, temperature, and humidity scales u_*, t_*, and q_* and a second based on the routine meteorological quantities U_h, $T_s - T_h$, and $Q_s - Q_h$. The subscript h here denotes the wind speed (U_h), temperature (T_h), or humidity (Q_h) at a reference height h; the subscript s indicates the surface value. I also develop analytical expressions for the coefficients A and B as functions of λ, the atmospheric pressure (P), and the temperature and the humidity in four wavelength regions: visible (including near infrared), an infrared window, near millimeter, and radio. In a sensitivity analysis of the two estimation procedures, the core of the paper, I demonstrate that the accuracy of the C_n^2 estimate is a strong function of the Bowen ratio (Bo). At two Bo values within the interval $[-10, 10]$, one dependent on λ and the other dependent on meteorological conditions, the uncertainty in the C_n^2 estimate becomes infinite.

1. INTRODUCTION

The refractive-index structure parameter C_n^2, defined from

$$\overline{[n(\mathbf{x}) - n(\mathbf{x} + \mathbf{r})]^2} = C_n^2 r^{2/3}, \tag{1.1}$$

is an important quantity in the study of electromagnetic wave propagation in the atmospheric surface layer. Here n is the turbulent refractive-index fluctuation, $\mathbf{x}$ and $\mathbf{x} + \mathbf{r}$ are two points in space, r is the magnitude of $\mathbf{r}$, and the overbar denotes a time average. C_n^2 is required in parameterizing theoretical studies,[1,2] for evaluating instrument design and performance,[3–5] and for analyzing field data.[6–9] For example, C_n^2 and the turbulence inner scale l_0 are the only two variables in the three-dimensional Tatarskii[10] spectrum for refractive-index fluctuations,

$$\Phi_{3n}(k) = 0.033 C_n^2 k^{-11/3} \exp(k^2/k_m^2), \tag{1.2}$$

where k is the three-dimensional turbulence wave number and $k_m = 5.92/l_0$. This spectrum is used frequently in modeling refractive-index turbulence and thus for evaluating how electro-optical systems interact with the turbulence.[1,4] In one dimension, Eq. (1.2) reduces in the inertial-convective subrange to

$$\Phi_{1n}(k_1) = 0.249 C_n^2 k_1^{-5/3}, \tag{1.3}$$

where k_1 is the one-dimensional wave number. This spectrum has been useful in describing measured refractive-index spectra.[9,11,12]

Because C_n^2 is fundamental to understanding electromagnetic wave propagation in the atmosphere, it would be useful to know how to estimate C_n^2 from measured or modeled meteorological quantities. Electro-optical systems could then be optimized beforehand for the C_n^2 climate likely to be encountered during a field deployment.

Friehe[11] and Davidson *et al.*[14] previously considered this problem and developed methods of estimating C_n^2 from meteorological measurements over the ocean. I consider here the problem of estimating C_n^2 over snow and snow-covered sea ice and expand on the analyses by Friehe and Davidson *et al.* in several ways. They considered light only in the visible; I look at four wavelength regions: (1) visible (to near infrared), 0.36–3 μm; (2) an infrared window, 7.8–19 μm; (3) near millimeter, 0.3–3 mm; and (4) radio waves, 3 mm to infinity. Friehe and Davidson *et al.* based their estimates of C_n^2 on the bulk meteorological quantities U_h, ΔT, and ΔQ, where U_h is the wind speed at a reference height h, ΔT is the potential temperature difference between the surface and the height h, and ΔQ is the analogous absolute humidity difference. I work with these bulk quantities, too, but also show how to estimate C_n^2 from u_*, t_*, and q_*, which are scales related to the vertical fluxes of momentum and sensible and latent heat, respectively. Although Davidson *et al.*, Wyngaard and Lemone,[15] and Kohsiek[16] hinted how to use u_*, t_*, and q_* to find C_n^2, I treat the problem explicitly and, most important, do a detailed sensitivity analysis of both methods of estimating C_n^2. This analysis shows that neither method yields C_n^2 accurately for all conditions; both methods for all four wavelength regions suffer from poor accuracy for some limited range of Bowen ratios. Friehe and Davidson *et al.* did no similar sensitivity analysis to my knowledge.

The methods that I develop are applicable to any horizontally homogeneous surface. I focus on snow and sea ice because the drag coefficient and the scalar roughness, which are necessary to relate C_n^2 to bulk meteorological quantities, have been evaluated for these surfaces and are fairly simple to parameterize.

2. RELATING REFRACTIVE INDEX TO METEOROLOGY

The instantaneous refractive index $\tilde{n}$ at an arbitrary electromagnetic wavelength λ is usually written as a function of the instantaneous atmospheric pressure $\tilde{p}$ (in hectopascals), the

0740-3232/88/040481-15$02.00

instantaneous temperature $\tilde{t}$ (in degrees Kelvin), and the instantaneous absolute humidity $\tilde{q}$ (in kilograms per cubic meter):

$$\tilde{n} = f(\lambda, \tilde{p}, \tilde{t}, \tilde{q}). \tag{2.1}$$

Doing a Reynolds decomposition of each of these variables, we write

$$\tilde{n} = N + n, \tag{2.2}$$

$$\tilde{p} = P + p, \tag{2.3}$$

$$\tilde{t} = T + t, \tag{2.4}$$

$$\tilde{q} = Q + q, \tag{2.5}$$

where on each line the uppercase variable is the ensemble average and the lowercase variable without the tilde is the zero-mean turbulent fluctuation about that mean.

Let us expand Eq. (2.1) as a multivariable Taylor series about average conditions. Assuming that the turbulent fluctuations are small compared with their respective means, we need keep only the first-order terms; consequently,

$$\tilde{n} = N + n = f(\lambda, P, T, Q) + \left(\frac{\partial f}{\partial \tilde{p}}\bigg|_{P,T,Q}\right)p + \left(\frac{\partial f}{\partial \tilde{t}}\bigg|_{P,T,Q}\right)t + \left(\frac{\partial f}{\partial \tilde{t}}\bigg|_{P,T,Q}\right)q. \tag{2.6}$$

Taking the ensemble or time average of Eq. (2.6), we see that, to first order,

$$N = f(\lambda, P, T, Q) \tag{2.7}$$

and

$$n = \left(\frac{\partial f}{\partial \tilde{p}}\bigg|_{P,T,Q}\right)p + \left(\frac{\partial f}{\partial \tilde{t}}\bigg|_{P,T,Q}\right)t + \left(\frac{\partial f}{\partial \tilde{q}}\bigg|_{P,T,Q}\right)q. \tag{2.8}$$

Gossard,[17] Friehe *et al.*,[11] Wesely,[18] Hill *et al.*,[19] and McBean and Elliott[20] all evaluated the contribution of the pressure term in Eq. (2.8), and all found it negligible in the atmosphere; therefore I simplify Eq. (2.8) to

$$n = A(\lambda, P, T, Q)t + B(\lambda, P, T, Q)q, \tag{2.9}$$

where

$$A = \frac{\partial f}{\partial \tilde{t}}\bigg|_{P,T,Q}, \tag{2.10}$$

$$B = \frac{\partial f}{\partial \tilde{q}}\bigg|_{P,T,Q}. \tag{2.11}$$

Because for a chosen electromagnetic wavelength and a given set of meteorological conditions A and B are constant, we see from Eq. (2.9) that turbulent fluctuations in the refractive index depend linearly on turbulent fluctuations in the temperature and the humidity. Equation (2.9) is thus the basis of any attempt to relate turbulence in the refractive index to meteorological parameters. We must therefore know A and B.

3. FINDING A AND B

Hill *et al.*[19] presented plots of A and B values over the wavelength continuum from 5.7 μm to radio wavelengths, but theirs were tedious line-by-line computations for one set of pressure, temperature, and humidity values. I want to find analytical expressions that will let us find A and B easily for arbitrary meteorological conditions. At present, four useful regions in the electromagnetic spectrum have yielded experimental data that satisfy Eq. (2.1). These are the visible region (including the near infrared), an infrared window, the near-millimeter region, and the radio region. I shall derive expressions for A and B in each of these regions.

A. Visible Region (Wavelengths from 0.36 to 3 μm)

According to Owens,[21] for visible and near-infrared wavelengths, 0.36–3 μm,[22] the instantaneous refractivity $10^6(\tilde{n}_v - 1)$ has contributions from dry air ($\tilde{n}_{vd}$) and from water vapor ($\tilde{n}_{vw}$):

$$10^6(\tilde{n}_v - 1) = \tilde{n}_{vd} + \tilde{n}_{vw}, \tag{3.1}$$

where the subscript v indicates visible and near-infrared wavelengths, and the subscripts d and w indicate contributions from dry air and water vapor. Owens gave

$$\tilde{n}_{vd} = m_1(\lambda)[(\tilde{p} - \tilde{e})/\tilde{t}], \tag{3.2}$$

$$\tilde{n}_{vw} = m_2(\lambda)(\tilde{e}/\tilde{t}), \tag{3.3}$$

where $\tilde{p}$ is the total instantaneous atmospheric pressure in hectopascals and $\tilde{e}$ is the instantaneous vapor pressure, also in hectopascals. The functions m_1 and m_2 are

$$m_1(\lambda) = 23.7134 + \frac{6839.397}{130 - \sigma^2} + \frac{45.473}{38.9 - \sigma^2}, \tag{3.4}$$

$$m_2(\lambda) = 64.8731 + 0.58058\sigma^2 - 0.0071150\sigma^4 + 0.0008851\sigma^6, \tag{3.5}$$

where

$$\sigma = \lambda^{-1} \tag{3.6}$$

for λ in micrometers. Combining Eqs. (3.1)–(3.3) gives

$$10^6(\tilde{n}_v - 1) = m_1(\lambda)(\tilde{p}/\tilde{t}) + [m_2(\lambda) - m_1(\lambda)](\tilde{e}/\tilde{t}). \tag{3.7}$$

From the ideal gas law,

$$\tilde{e} = 10^{-2}\tilde{q}\tilde{t}R/M_w, \tag{3.8}$$

where R (= 8.31441 J K^{-1} mol^{-1}) is the universal gas constant and M_w (= 18.0160 × 10^{-3} kg mol^{-1}) is the molecular weight of water. Thus $\tilde{e} = 4.6150\tilde{q}\tilde{t}$, and Eq. (3.7) becomes

$$10^6(\tilde{n}_v - 1) = m_1(\lambda)(\tilde{p}/\tilde{t}) + 4.6150\,[m_2(\lambda) - m_1(\lambda)]\tilde{q}. \tag{3.9}$$

Applying Eqs. (2.10) and (2.11) to Eq. (3.9), we find that

$$A_v = -10^{-6}\, m_1(\lambda)(P/T^2), \tag{3.10}$$

$$B_v = 4.6150 \times 10^{-6}[m_2(\lambda) - m_1(\lambda)]. \tag{3.11}$$

At a wavelength of 0.55 μm, for example, $A_v = 79.0 \times 10^{-6}$ (P/T^2), and $B_v = -56.4 \times 10^{-6}$.

B. Infrared Window (Wavelengths from 7.8 to 19 μm)

Hill and Lawrence[22] developed an empirical expression for the refractivity $\tilde{n}_{iw}$ that is due to water vapor in the infrared window between 7.8 and 19 μm. With their function, the total instantaneous refractivity in that region is

$$10^6(\tilde{n}_i - 1) = \tilde{n}_{vd} + \tilde{n}_{iw}, \tag{3.12}$$

where Eq. (3.2) gives the dry-air contribution $\tilde{n}_{vd}$.[21] From Eq. (3.8), Eq. (3.12) becomes

$$10^6(\tilde{n}_i - 1) = m_1(\lambda)(\tilde{p}/\tilde{t}) - 4.6150 m_1(\lambda)\tilde{q} + \tilde{n}_{iw}. \quad (3.13)$$

For temperatures between −40 and 40°C, Hill and Lawrence gave

$$\tilde{n}_{iw} = \tilde{q}\left[\frac{957 - 928\tilde{\theta}^{0.4}(\chi - 1)}{1.03\tilde{\theta}^{0.17} - 19.8\chi^2 + 8.2\chi^4 - 1.7\chi^8} + \frac{3.747 \times 10^6}{12499 - \chi^2}\right], \quad (3.14)$$

where

$$\tilde{\theta} = \tilde{t}/273.16K, \quad (3.15)$$

$$\chi = (10\ \mu\text{m})/\lambda. \quad (3.16)$$

Note that their Eq. (14) contains two typographical errors that are corrected in Eq. (3.14) here.

We see from Eqs. (3.13), (3.14), (2.10), and (2.11) that in this spectral region the A and B values have both dry-air (A_{vd} and B_{vd}) and water-vapor (A_{iw} and B_{iw}) contributions; that is,

$$A_i = A_{vd} + A_{iw}, \quad (3.17)$$

$$B_i = B_{vd} + B_{iw}. \quad (3.18)$$

From Eqs. (2.10), (2.11), and (3.13),

$$A_{vd} = -10^{-6} m_1(\lambda)(P/T^2), \quad (3.19)$$

$$B_{vd} = -4.6150 \times 10^{-6} m_1(\lambda). \quad (3.20)$$

Similarly, the water-vapor contributions are

$$A_{iw} = 10^{-6}Q\{-1.359\theta^{-0.6}(\chi - 1)H^{-1} - [0.6135\theta^{-0.83} + 0.5949\theta^{-0.43}(\chi - 1)]H^{-2}\}, \quad (3.21)$$

$$B_{iw} = 10^{-6}[957 - 928\theta^{0.4}(\chi - 1)]H^{-1} + 3.747/(12449 - \chi^2), \quad (3.22)$$

where

$$\theta = T/273.16K, \quad (3.23)$$

$$H = 1.03\theta^{0.17} - 19.8\chi^2 + 8.2\chi^4 - 1.7\chi^8. \quad (3.24)$$

C. Radio Region (Wavelengths Greater Than 3 mm)

For radio wavelengths from infinity down to roughly 3 mm, the total instantaneous refractivity is the sum of dry-air contributions ($\tilde{n}_{rd}$) and water-vapor resonances in the infrared ($\tilde{n}_{rw}$),

$$10^6(\tilde{n}_r - 1) = \tilde{n}_{rd} + \tilde{n}_{rw}, \quad (3.25)$$

where the subscript r refers to radio waves. Hill *et al.*,[23] who referred to Boudouris[24] for the values of the coefficients, gave

$$\tilde{n}_{rd} = 77.6(\tilde{p} - \tilde{e})/\tilde{t}, \quad (3.26)$$

$$\tilde{n}_{rw} = 72.0(\tilde{e}/\tilde{t}) + 0.375 \times 10^6(\tilde{e}/\tilde{t}^2). \quad (3.27)$$

Notice that these coefficients are identical to those recommended by Bean and Dutton.[25] Using Eq. (3.8) as before, we convert Eqs. (3.26) and (3.27) into

$$\tilde{n}_{rd} = 77.6(\tilde{p}/\tilde{t}) - 358\tilde{q}, \quad (3.28)$$

$$\tilde{n}_{rw} = (332 + 1.73 \times 10^6/\tilde{t})\tilde{q}. \quad (3.29)$$

Thus A and B again have both air-dry (A_{rd} and B_{rd}) and water-vapor (A_{rw} and B_{rw}) contributions. From Eqs. (2.10), (2.11), (3.28), and (3.29) we find that these are

$$A_{rd} = -77.6 \times 10^{-6}(P/T^2), \quad (3.30)$$

$$B_{rd} = -358 \times 10^{-6}, \quad (3.31)$$

$$A_{rw} = -1.73(Q/T^2), \quad (3.32)$$

$$B_{rw} = 332 \times 10^{-6} + 1.73/T. \quad (3.33)$$

Hence

$$A_r = -(77.6 \times 10^{-6}P + 1.73Q)/T^2, \quad (3.34)$$

$$B_r = -26 \times 10^{-6} + 1.73/T, \quad (3.35)$$

where for all practical purposes

$$B_r = 1.73/T. \quad (3.36)$$

Note that the refractive index for ratio waves is nondispersive: it has no dependence on wavelength [see Eqs. (3.26) and (3.27)]. The A_r and B_r values are therefore also independent of the wavelength.

D. Near-Millimeter Region (Wavelengths from 0.3 to 3 mm)

Specifying the refractivity is more difficult for the near-millimeter region than for the preceding three regions because it results from contributions from three sources: (1) the nondispersive radio refractivity ($\tilde{n}_{rd}$ and $\tilde{n}_{rw}$), (2) water-vapor resonances at wavelengths of <0.3 mm ($\tilde{n}_{mw1}$), and (3) water-vapor resonances at wavelengths of >0.3 mm ($\tilde{n}_{mw2}$).[26] That is, for wavelengths between 0.3 and 3 mm (or frequencies between 100 and 1000 GHz), the instantaneous refractivity is

$$10^6(\tilde{n}_m - 1) = \tilde{n}_{rd} + \tilde{n}_{rw} + \tilde{n}_{mw1} + \tilde{n}_{mw2}. \quad (3.37)$$

Hill[26] evaluated the $\tilde{n}_{mw1}$ and $\tilde{n}_{mw2}$ terms, and although the $\tilde{n}_{mw2}$ term requires a line-by-line summation of the resonances and consequently does not have simple analytical form, he did derive an analytical approximation for $\tilde{n}_{mw1}$:

$$\tilde{n}_{mw1} = \tilde{q}\sum_{j=1}^{4} \alpha_j(296/\tilde{t})^{a_j}[1 - \beta_j(296/\tilde{t})](0.303/\lambda)^{2j}. \quad (3.38)$$

Table 1 gives the constants α_j, a_j, and β_j; all quantities in Eq. (3.38) are, as usual, in mks units except the wavelength λ, which must be in millimeters.

For the sake of an analytic solution, I will ignore the $\tilde{n}_{mw2}$ contribution to Eq. (3.37). This, of course, means that I am no longer modeling the refractivity accurately throughout

Table 1. The Coefficients in Eq. (3.38)

j	α_j	a_j	β_j
1	1.382221×10^3	1.650000	0.1993324
2	-0.2135129×10^3	0.1619430	3.353494
3	-0.1485997×10^3	0.1782352	3.100942
4	-0.1088790×10^3	0.1918662	3.004944

the near-millimeter region. In particular, around the resonances at 0.303, 0.399, and 0.538 mm (988, 752, and 557 GHz),[26,27] the abbreviated model is not good. However, it should be accurate to ±10% in the window regions 0.31–0.34 mm (880–970 GHz), 0.42–0.44 mm (680–720 GHz), and 0.83–3 mm (100–360 GHz). These windows seem to be where most current millimeter-wavelength turbulence measurements are being made.[27–29]

Because of the three terms remaining in Eq. (3.37), the millimeter-wavelength A and B values each have three terms:

$$A_m = A_{rd} + A_{rw} + A_{mw1}, \tag{3.39}$$

$$B_m = B_{rd} + B_{rw} + B_{mw1}. \tag{3.40}$$

A_{rd}, A_{rw}, B_{rd}, and B_{rw} are the nondispersive radio-wave contributions evaluated in Subsection 3.C, Eqs. (3.34) and (3.36). A_{mw1} and B_{mw1} are derived from Eqs. (2.10), (2.11), and (3.38):

$$A_{mw1} = 10^{-6}(Q/T)\sum_{j=1}^{4}\alpha_j(296/T)^{a_j}(0.303/\lambda)^{2j} \times [-a_j + \beta_j(296/T)(1 + a_j)], \tag{3.41}$$

$$B_{mw1} = 10^{-6}\sum_{j=1}^{4}\alpha_j(296/T)^{a_j}[1 - \beta_j(296/T)](0.303/\lambda)^{2j}. \tag{3.42}$$

4. MONIN-OBUKHOV SIMILARITY OF C_n^2

Over a horizontally homogeneous surface in steady-state conditions, an atmospheric surface layer exists up to heights of 10–50 m, depending on the height of the planetary boundary layer. In the surface layer the vertical fluxes of momentum ($-\overline{uw}$), sensible heat ($\overline{wt}$), and the latent heat ($\overline{wq}$) are constant with height. Consequently, it is possible to define velocity (u_*, the friction velocity), temperature (t_*), and humidity (q_*) scales that are also constant with height:

$$u_*^2 = -\overline{uw}, \tag{4.1}$$

$$u_* t_* = -\overline{wt}, \tag{4.2}$$

$$u_* q_* = -\overline{wq}. \tag{4.3}$$

Here u and w are turbulent fluctuations in the longitudinal and vertical velocities, defined as t and q were in Eqs. (2.4) and (2.5). These velocity, temperature, and humidity scales, in turn, yield a length scale, the Obukhov length L,[30] that is also constant with height:

$$L^{-1} = \frac{\gamma\kappa}{u_*^2\overline{T}}\left(t_* + \frac{0.61\overline{T}}{\rho + 0.61\overline{Q}}q_*\right). \tag{4.4}$$

Here γ is the acceleration of gravity, κ is von Kármán's constant (0.4), $\overline{T}$ and $\overline{Q}$ are representative values of the temperature and the absolute humidity in the surface layer, and ρ is the density of moist air.

According to Monin–Obukhov similarity theory,[31–34] any surface-layer meteorological quantity, when properly scaled with u_*, t_*, q_*, L, the measurement height z, and the buoyancy parameter $\gamma/\overline{T}$, should be a universal function of the stability parameter $\zeta = z/L$. For example, the vertical gradients of average wind speed $U(z)$, potential temperature $T(z)$, and absolute humidity $Q(z)$ have been found to satisfy Monin–Obukhov similarity[35–38]:

$$\frac{\partial U(z)}{\partial z} = \frac{u_*}{\kappa z}\phi_m(\zeta), \tag{4.5}$$

$$\frac{\partial T(z)}{\partial z} = \frac{t_*}{\kappa z}\phi_h(\zeta), \tag{4.6}$$

$$\frac{\partial Q(z)}{\partial z} = \frac{q_*}{\kappa z}\phi_w(\zeta). \tag{4.7}$$

The functions ϕ_m, ϕ_h, and ϕ_w must be found experimentally. Although there is no consensus yet on their forms, the measurements seem to be converging toward the functions used by Large and Pond[34–40]:

for unstable conditions ($\zeta < 0$)

$$\phi_m(\zeta) = (1 - 16\zeta)^{-1/4}, \tag{4.8}$$

$$\phi_h(\zeta) = \phi_w(\zeta) = (1 - 16\zeta)^{-1/2}; \tag{4.9}$$

for stable conditions ($\zeta > 0$)

$$\phi_m(\zeta) = \phi_h(\zeta) = \phi_w(\zeta) = 1 + 7\zeta. \tag{4.10}$$

Paulson[41] showed how to integrate Eqs. (4.5)–(4.7) with the empirical functions [Eqs. (4.8)–(4.10)] to get expressions for the profiles of wind speed, temperature, and humidity:

$$U(z) = (u_*/\kappa)[\ln(z/z_0) - \psi_m(\zeta)], \tag{4.11}$$

$$T(z) = T_s + (t_*/\kappa)[\ln(z/z_T) - \psi_h(\zeta)], \tag{4.12}$$

$$Q(z) = Q_s + (q_*/\kappa)[\ln(z/z_Q) - \psi_h(\zeta)]. \tag{4.13}$$

In these expressions, z_0 is the familiar roughness length for wind speed; z_T and z_Q are the roughness lengths for temperature and humidity, the so-called scalar roughness lengths. z_0 is the height at which the semilogarithmic wind-speed profile extrapolates to $U = 0$. Similarly, z_T and z_Q are the heights at which the semilogarithmic temperature and humidity profiles extrapolate to their surface values, T_s and Q_s, respectively. For unstable conditions ($\zeta < 0$)

$$\psi_m(\zeta) = 2\ln[(1 + x)/2] + \ln[(1 + x^2)/2] - \arctan(x) + \pi/2, \tag{4.14}$$

$$\psi_h(\zeta) = 2\ln[(1 + x^2)/2], \tag{4.15}$$

where

$$x = (1 - 16\zeta)^{1/4}. \tag{4.16}$$

For stable conditions ($\zeta > 0$)

$$\psi_m(\zeta) = \psi_h(\zeta) = -7\zeta. \tag{4.17}$$

Other quantities also yield to similarity arguments. For example, Wyngaard *et al.*[42] showed that the structure parameter for temperature, C_t^2, which is defined as C_n^2 in Eq. (1.1) or Eq. (1.3), should have a universal form when properly scaled. They obtained

$$\frac{z^{2/3}C_t^2}{t_*^2} = g_t(\zeta), \tag{4.18}$$

where the similarity function that was given by Wyngaard[33] but was modified to reflect a value of 0.4 for the von Kármán constant is

$$g_t(\zeta) = 4.9(1 - 6.1\zeta)^{-2/3} \quad \text{for } \zeta \le 0 \tag{4.19a}$$

$$= 4.9(1 + 2.2\zeta^{2/3}) \quad \text{for } \zeta \ge 0. \tag{4.19b}$$

Fairall *et al.*[43] and Kohsiek[16] extended these arguments to the humidity structure parameter C_q^2 and to the temperature–humidity structure parameter C_{tq}, obtaining

$$\frac{z^{2/3}C_q^{\,2}}{q_*^{\,2}} = g_q(\zeta), \tag{4.20}$$

$$\frac{z^{2/3}C_{tq}}{t_*q_*} = g_{tq}(\zeta). \tag{4.21}$$

These similarity relations suggest that C_n^2 also exhibits Monin–Obukhov similarity. From Eqs. (1.1) and (2.9) we see that

$$C_n^{\,2} = A^2C_t^{\,2} + 2ABC_{tq} + B^2C_q^{\,2}. \tag{4.22}$$

Also, because from Eqs. (2.9), (4.2), and (4.3) we can write

$$\overline{wn} = A\overline{wt} + B\overline{wq}, \tag{4.23}$$

it is possible to define a refractive-index scale n_* that is similar to the temperature and humidity scales,

$$n_* = At_* + Bq_*. \tag{4.24}$$

Thus we would expect from similarity theory that

$$\frac{z^{2/3}C_n^{\,2}}{n_*^{\,2}} = g_n(\zeta). \tag{4.25}$$

There have, however, been no experimental attempts to verify Eq. (4.25) at wavelengths other than in the visible or near-infrared region, where C_n^2 is virtually $A^2C_t^2$. On the basis of Eq. (4.22), we can nevertheless speculate on how C_n^2 will behave at infrared, near-millimeter, and radio wavelengths, since we know A and B at these wavelengths and have some information on the behavior of C_q^2 and C_{tq}.

The variance budgets for temperature, humidity, and refractive index and the temperature–humidity covariance budget have virtually identical forms[44]:

$$\frac{2u_*t_*^{\,2}\phi_h(\zeta)}{\kappa z} = N_t, \tag{4.26a}$$

$$\frac{2u_*q_*^{\,2}\phi_h(\zeta)}{\kappa z} = N_q, \tag{4.26b}$$

$$\frac{2u_*n_*^{\,2}\phi_h(\zeta)}{\kappa z} = N_n, \tag{4.26c}$$

$$\frac{2u_*t_*q_*\phi_h(\zeta)}{\kappa z} = N_{tq}, \tag{4.26d}$$

where N_t, N_q, N_n and N_{tq} are the respective dissipation rates. Note that in writing Eqs. (4.26), I ignored the vertical turbulent transport term in each equation; this makes the equality in each accurate only to within ±10%.[44]

The scalar dissipation rates are related to the structure parameters by

$$\beta_tN_t\epsilon^{-1/3} = 0.249C_t^{\,2}, \tag{4.27a}$$

$$\beta_qN_q\epsilon^{-1/3} = 0.249C_q^{\,2}, \tag{4.27b}$$

$$\beta_nN_n\epsilon^{-1/3} = 0.249C_n^{\,2}, \tag{4.27c}$$

$$\beta_{tq}N_{tq}\epsilon^{-1/3} = 0.249C_{tq}^{\,2}, \tag{4.27d}$$

where ϵ is the dissipation rate of turbulent kinetic energy, and the β's are the Kolmogorov constants. The best experimental data have not established any significant difference among the β values; I therefore use $\beta_t = \beta_q = \beta_n = \beta_{tq} = \beta = 0.4$.[44]

The turbulent kinetic-energy dissipation rate also exhibits Monin–Obukhov similarity:

$$\epsilon = \frac{u_*^{\,3}}{\kappa z}\phi_\epsilon(\zeta), \tag{4.28}$$

where ϕ_ϵ has been found to be[45–48]

$$\phi_\epsilon(\zeta) = [1 + 0.46(-\zeta)^{2/3}]^{3/2} \quad \text{for } -2 \le \zeta \le 0 \tag{4.29a}$$

$$= [1 + 2.3\zeta^{3/5}]^{3/2} \quad \text{for } 0 \le \zeta \le 2. \tag{4.29b}$$

Again, I have modified the constants (i.e., 0.46 and 2.3) to reflect a von Kármán constant of 0.4.

From Eqs. (4.27)–(4.29), we see that each of Eqs. (4.26) reduces to the same form,

$$\frac{z^{2/3}C_t^{\,2}}{t_*^{\,2}} = \frac{z^{2/3}C_q^{\,2}}{q_*^{\,2}} = \frac{z^{2/3}C_n^{\,2}}{n_*^{\,2}} = \frac{z^{2/3}C_{tq}}{t_*q_*}$$

$$= \frac{2\beta\phi_h(\zeta)}{0.249\kappa^{2/3}\phi_\epsilon(\zeta)^{1/3}} = \frac{5.92\phi_h(\zeta)}{\phi_\epsilon(\zeta)^{1/3}} \equiv g_b(\zeta), \tag{4.30}$$

where the subscript b indicates that the function is derived from the budget equations. Panofsky and Dutton[34] derived virtually the same form for C_t^2.

One shortcoming of g_b is that it does not have the proper z dependence at large $|\zeta|$. Equation (4.30) shows $g_b \propto z^{-5/6}$ at large $-\zeta$ and $g_b \propto z^{7/10}$ at large ζ, while the accepted dependences are $g \propto z^{-2/3}$ and $g \propto z^{2/3}$, respectively.[33] This inconsistency, however, is not an indictment of the theoretical steps that led to Eq. (4.30) but rather is evidence that ϕ_ϵ needs to be investigated further for large $|\zeta|$ values. For example, if

$$\phi_\epsilon(\zeta) = (1 - 3\zeta)^{1/2} \quad \text{for } \zeta \le 0 \tag{4.31a}$$

$$= 1 + 6\zeta \quad \text{for } \zeta \ge 0, \tag{4.31b}$$

relations similar to Eqs. (4.29) for their region of validity, $-2 \le \zeta \le 2$, then g_b would have the theoretically correct z dependence at large $|\zeta|$. Notice that Eq. (4.31b) is the production-equals-dissipation form of the turbulent kinetic-energy budget that Large and Pond[39] used.

In Fig. 1, Wyngaard's[33] structure parameter function [Eq. (4.19)] and the budget-based function [Eq. (4.30)] are plotted with Eqs. (4.9) and (4.10) for ϕ_h and with Eqs. (4.29) for ϕ_ϵ. Kohsiek[16] also found $z^{2/3}C_t^2/t_*^{\,2}$, $z^{2/3}C_q^{\,2}/q_*^{\,2}$, and $z^{2/3}C_{tq}/t_*q_*$ experimentally for $\zeta \le -0.2$; Fig. 1 shows his result for temperature:

$$\frac{z^{2/3}C_t^{\,2}}{t_*^{\,2}} = 1.21(-\zeta)^{-2/3} \quad \text{for } \le -0.02. \tag{4.32}$$

Davidson *et al.*[49] corroborated Wyngaard's[33] expression for g_t, Eqs. (4.19), with C_t^2 data in the interval $-20 \le \zeta \le 1$, and Kunkel *et al.*[50] corroborated it in the interval $-20 \le \zeta$

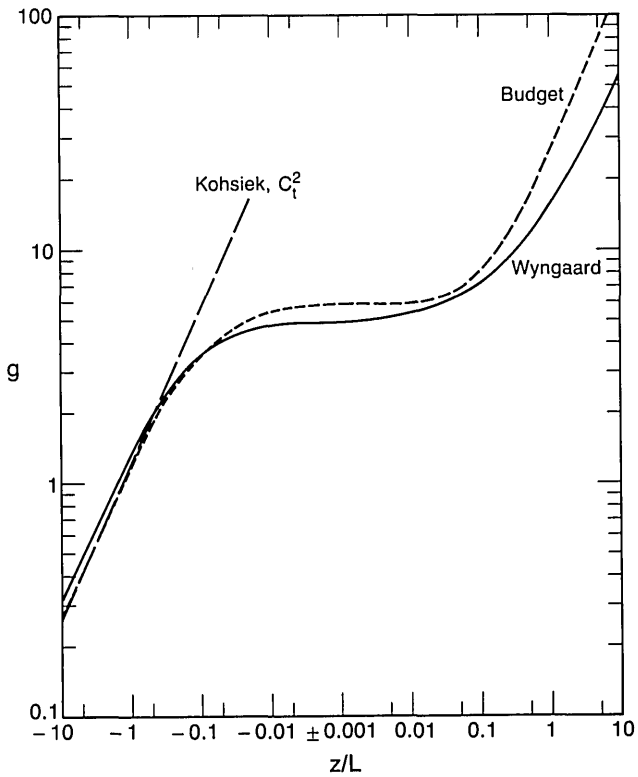

Fig. 1. The nondimensional structure parameter $g(\zeta)$ according to Wyngaard[33] [Eqs. (4.19)]; derived from the scalar variance budget, [Eq. (4.29) with Eqs. (4.9) and (4.10) for ϕ_h and with Eq. (4.30) for ϕ_ϵ]; and as found experimentally by Kohsiek[16] for C_t^2 [Eq. (4.32)].

≤ -0.1; but their data and those on which Wyngaard *et al.*[42] originally based Eqs. (4.19) are too scattered to rule out the possibility that Eq. (4.30) may also be a correct model for C_t^2, at least. Panofsky and Dutton[34] reached this same conclusion. Consequently, both Eqs. (4.19) and Eq. (4.30) are reasonable models for $-10 \leq \zeta \leq 1$, the stability range where most of the C_t^2 data have been collected.

The result obtained by Kohsiek[16] [Eq. (4.32)] is therefore suspect. As Fig. 1 shows, he found the proper dependence on ζ at large $-\zeta$ that is, $(-\zeta)^{-2/3}$, but this dependence continued up to $\zeta = -0.02$, whereas the Wyngaard and budget results flatten out much sooner. Kohsiek's results for C_q^2 and C_{tq} also behave as in Eq. (4.32) but with different multiplicative constants for each. Equation (4.30), however, shows that these structure functions, too, should break from the $(-\zeta)^{-2/3}$ slope much sooner than Kohsiek found. I speculate that perhaps his experimental site, Table Mountain, which is near Boulder, Colorado, suffered from nonhomogeneity. Table Mountain is a mesa 3 km across that is elevated roughly 50 m above the surrounding terrain. It is also just 3–4 miles (approximately 4–6 km), generally downwind, from the foothills of the Colorado Front Range. Although the top of the mesa, where Kohsiek made his measurements, is fairly smooth and level, the precipitous sides, the proximity of the mountains, and the comparison of his results with others (Fig. 1) lead me to believe either that his measurements do not represent horizontally homogeneous conditions or that at his site the vertical transport terms that I ignored in Eqs. (4.26) were not small, as is commonly assumed.[44,51]

In summary, the C_t^2 measurements of Wyngaard *et al.*,[42] Davidson *et al.*,[49] and Kunkel *et al.*[50] agree that Eqs. (4.19) are an accurate model for $z^{2/3}C_t^2/t_*^2$ but are too scattered for us to reject Eq. (4.30) as an equally viable model. Therefore, because the q and n variance budgets and the t–q covariance budget all also lead to Eq. (4.30), it is reasonable to conclude that

$$g_t(\zeta) = g_q(\zeta) = g_{tq}(\zeta) = g_n(\zeta) \equiv g(\zeta), \tag{4.33}$$

where g is given by Eqs. (4.19). Notice that if $g_t(\zeta) = g_q(\zeta) = g_{tq}(\zeta) = g(\zeta)$, then also $g_n(\zeta) = g(\zeta)$ by virtue of Eq. (4.22). I therefore take Eq. (4.25) as an accurate model for C_n^2 in the atmospheric surface layer.

5. ESTIMATING C_n^2 FROM THE TURBULENT FLUXES

From Eq. (4.26),

$$C_n^2 = z^{-2/3} n_*^2 g(\zeta); \tag{5.1}$$

C_n^2 is therefore related to the turbulent surface fluxes of momentum (u_*^2) and sensible ($-u_* t_*$) and latent ($-u_* q_*$) heat by virtue of Eq. (4.24). Consequently, with measurements of the surface fluxes and of ambient conditions (namely, P, T, and Q needed to find A, B, and z/L), we can estimate C_n^2 at an arbitrary height z within the atmospheric surface layer.

It may, however, be unnecessary to know both t_* and q_* to make an accurate estimate of n_*. We can rewrite Eq. (4.24) as

$$\frac{n_*}{At_*} = 1 + \frac{Bq_*}{At_*}. \tag{5.2}$$

Next we define the Bowen ratio Bo, which is the ratio of sensible heat flux to latent heat flux:

$$\mathrm{Bo} = \frac{-\rho c_p u_* t_*}{-L_s u_* q_*} = \frac{\rho c_p}{L_s}\frac{t_*}{q_*} = \frac{t_*}{Kq_*}, \tag{5.3}$$

where c_p is the specific heat of air at constant pressure, L_s is the latent heat of sublimation of ice, and K is a constant, near 2100 $\mathrm{m^3\ K\ kg^{-1}}$, for a given set of ambient conditions. Substituting Eq. (5.3) into Eq. (5.2) yields

$$\frac{n_*}{At_*} = 1 + \frac{B}{KA\ \mathrm{Bo}}. \tag{5.4}$$

This equation indicates whether t_* or q_* is the dominant term in Eq. (4.24). Clearly, the result depends on the electromagnetic wavelength, i.e., the A and B values, and on the Bowen ratio. If n_*/At_* is near 1, then n_* depends negligibly on q_*; but if $|n_*/At_*|$ is large, then q_* rather than t_* makes the dominant contribution to n_*.

Figure 2 shows plots of n_*/At_* as a function of the Bowen ratio for four electromagnetic wavelengths. The A and B values used in Eq. (5.4) were computed from the equations developed in Section 3. From the figure we see that when |Bo| is large, i.e., when the sensible heat flux is dominant, n_*/At_* is near 1 for all wavelengths; the t_* term is thus the dominant contributor in Eq. (4.24). On the other hand, when |Bo| is small and the latent heat flux is dominant, $|n_*/At_*|$ is large for all wavelengths; the q_* term is then the dominant contributor in Eq. (4.24). In the midregions, for

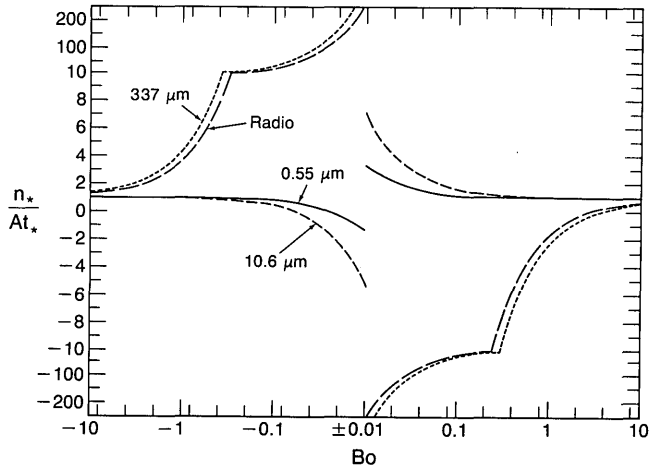

Fig. 2. Dependence of the refractive-index scale on the temperature and humidity scales for four electromagnetic wavelengths. Atmospheric conditions are typical for a snow or sea ice surface: P = 1000 hPa, $T = -10°C$, $Q = 1.93 \times 10^{-3}$ kg m^{-3} (i.e., relative humidity of 90%). A wavelength of 337 μm corresponds to a frequency of 890 GHz. Notice that the n_*/At_* axis changes scale at ±10.

|Bo| values between 0.1 and 1, t_* dominates for visible and infrared wavelengths, while q_* dominates for near-millimeter and radio wavelengths. Thus we cannot say unequivocally that for a given wavelength either temperature or humidity will dominate the refractive-index fluctuations: The partitioning also depends on the Bowen ratio.

Because the Bowen ratio is so important for interpreting Fig. 2 and for many figures to follow, it is useful to review a few Bo measurements over snow and sea ice. Measurements of turbulent surface fluxes over snow generally show the Bowen ratio to be negative: the snow gains sensible heat from the air but loses latent heat by sublimation. Hicks and Martin[52] found Bo between −1 and −0.2 in four measurements over a snow surface near the melting point. At lower air temperatures, Yelagina *et al.*[53] found Bo to be typically −5 to −1 for many measurements over snow, and Andreas[9] found it to be −3 to −1. In stationary atmospheric conditions, McKay and Thurtell[54] also observed this general range, from −4 to −1, but measured Bowen ratios between 1 and 4 during warm-air advection that fostered downward surface fluxes of both sensible and latent heat. Over sea ice the Bowen ratio tends to be positive because of the oceanic heat transferred through the ice. Over compact, snow-covered Arctic sea ice, Thorpe *et al.*[55] measured Bo generally between 1 and 20. Over Antarctic sea ice with roughly 10% open water present, Andreas and Makshtas[56] obtained Bo values around 1. In summary, values of the Bowen ratio over snow-covered ground and over sea ice are commonly in the vicinities of −1 and 1, respectively.

To evaluate how good Eq. (5.1) really is for estimating C_n^2, we must know how sensitive C_n^2 is to the required input measurements z, u_*, t_*, and q_*. Using Eq. (4.24) in Eq. (5.1), we find that

$$C_n^2 = z^{-2/3} g(\zeta)(A^2 t_*^2 + 2ABt_* q_* + B^2 q_*^2). \tag{5.5}$$

Thus C_n^2 is a known function of z, ζ, t_*, and q_*; but ζ is, in turn, a known function of z, u_*, t_*, and q_* [see Eq. (4.4)]. Notice that I am ignoring the weak dependence of A, B, and L on P, T, and Q because these are assumed to be virtually constant over the time scales of interest. On identifying the independent variables, we can evaluate how sensitive a C_n^2 estimate is to them.

According to Eq. (5.5), a differential change in z, ζ, t_*, or q_* will result in a differential change in C_n^2 that obeys

$$dC_n^2 = \frac{\partial C_n^2}{\partial z} dz + \frac{\partial C_n^2}{\partial \zeta} d\zeta + \frac{\partial C_n^2}{\partial t_*} dt_* + \frac{\partial C_n^2}{\partial q_*} dq_*. \tag{5.6}$$

However, because ζ is a function of the independent variables z, u_*, t_*, and q_*,

$$d\zeta = \frac{\partial \zeta}{\partial z} dz + \frac{\partial \zeta}{\partial u_*} du_* + \frac{\partial \zeta}{\partial t_*} dt_* + \frac{\partial \zeta}{\partial q_*} dq_*. \tag{5.7}$$

Substituting this expression into Eq. (5.6) yields a sensitivity equation in terms of the true independent variables,

$$\begin{aligned} \frac{dC_n^2}{C_n^2} = {} & \frac{z}{C_n^2}\left[\frac{\partial C_n^2}{\partial z} + \frac{\partial C_n^2}{\partial \zeta}\frac{\partial \zeta}{\partial z}\right]\frac{dz}{z} + \frac{u_*}{C_n^2}\left[\frac{\partial C_n^2}{\partial \zeta}\frac{\partial \zeta}{\partial u_*}\right]\frac{du_*}{u_*} \\ & + \frac{t_*}{C_n^2}\left[\frac{\partial C_n^2}{\partial t_*} + \frac{\partial C_n^2}{\partial \zeta}\frac{\partial \zeta}{\partial t_*}\right]\frac{dt_*}{t_*} \\ & + \frac{q_*}{C_n^2}\left[\frac{\partial C_n^2}{\partial q_*} + \frac{\partial C_n^2}{\partial \zeta}\frac{\partial \zeta}{\partial q_*}\right]\frac{dq_*}{q_*}. \end{aligned} \tag{5.8}$$

Notice that I have divided through by C_n^2 to get the relative change dC_n^2/C_n^2 and have formed similar relative changes of the independent variables on the right-hand side of Eq. (5.8). These relative changes can also be interpreted as the relative uncertainties in the measurements of z, u_*, t_*, and q_* and in the resulting estimate of C_n^2. Therefore the coefficients multiplying these uncertainties predict how sensitive the estimated quantity C_n^2 is to uncertainties in the measured quantities. They are sensitivity coefficients.

Letting S denote a sensitivity coefficient, I rewrite Eq. (5.8) as

$$\begin{aligned} \frac{dC_n^2}{C_n^2} = {} & S_z(dz/z) + S_{u_*}(du_*/u_*) \\ & + S_{t_*}(dt_*/t_*) + S_{q_*}(dq_*/q_*). \end{aligned} \tag{5.9}$$

Defining ζ from Eq. (4.4) as $\zeta = z/L$, and using the Bowen ratio [Eq. (5.3)] to separate ζ into contributions owing to fluctuations in temperature (ζ_T) and humidity (ζ_Q),[31] we have

$$\zeta = \zeta_T + \zeta_Q = \frac{\gamma \kappa z t_*}{u_*^2 \overline{T}}\left(1 + \frac{0.61\overline{T}}{\rho + 0.61\overline{Q}}\frac{1}{K\,\mathrm{Bo}}\right), \tag{5.10}$$

$$= \zeta_T\left(1 + \frac{0.61\overline{T}}{\rho + 0.61\overline{Q}}\frac{1}{K\,\mathrm{Bo}}\right). \tag{5.11}$$

With these and with Eqs. (4.19) substituted for $g(\zeta)$ in Eq. (5.5), we can find the sensitivity coefficients in Eqs. (5.8) and (5.9):

$$S_z \equiv \frac{z}{C_n^2}\left(\frac{\partial C_n^2}{\partial z} + \frac{\partial C_n^2}{\partial \zeta}\frac{\partial \zeta}{\partial z}\right) \tag{5.12a}$$

$$= \frac{2}{3}\left(-1 + \frac{6.1\zeta}{1 - 6.1\zeta}\right) \qquad \text{for } \zeta \le 0 \tag{5.12b}$$

$$= \frac{2}{3}\left(-1 + \frac{2.2\zeta^{2/3}}{1 + 2.2\zeta^{2/3}}\right) \qquad \text{for } \zeta \ge 0; \tag{5.12c}$$

$$S_{u_*} \equiv \frac{u_*}{C_n^2}\left(\frac{\partial C_n^2}{\partial \zeta}\frac{\partial \zeta}{\partial u_*}\right), \tag{5.13a}$$

$$= \frac{-(4/3)(6.1)\zeta}{1-6.1\zeta} \quad \text{for } \zeta \le 0, \tag{5.13b}$$

$$= \frac{-(4/3)(2.2)\zeta^{2/3}}{1+2.2\zeta^{2/3}} \quad \text{for } \zeta \ge 0; \tag{5.13c}$$

$$S_{t_*} \equiv \frac{t_*}{C_n^2}\left(\frac{\partial C_n^2}{\partial t_*}+\frac{\partial C_n^2}{\partial \zeta}\frac{\partial \zeta}{\partial t_*}\right), \tag{5.14a}$$

$$= \frac{2}{1+(B/KA\mathrm{Bo})}+\frac{(2/3)(6.1)\zeta_T}{1-6.1\zeta} \quad \text{for } \zeta \le 0 \tag{5.14b}$$

$$= \frac{2}{1+(B/KA\mathrm{Bo})}+\frac{(2/3)(2.2)\zeta_T\zeta^{-1/3}}{1+2.2\zeta^{2/3}} \quad \text{for } \zeta \ge 0; \tag{5.14c}$$

$$S_{q_*} \equiv \frac{q_*}{C_n^2}\left(\frac{\partial C_n^2}{\partial q_*}+\frac{\partial C_n^2}{\partial \zeta}\frac{\partial \zeta}{\partial q_*}\right) \tag{5.15a}$$

$$= \frac{2B/KA\mathrm{Bo}}{1+(B/KA\mathrm{Bo})}+\frac{(2/3)(6.1)\zeta_Q}{1-6.1\zeta} \quad \text{for } \zeta \le 0 \tag{5.15b}$$

$$= \frac{2B/KA\mathrm{Bo}}{1+(B/KA\mathrm{Bo})}+\frac{(2/3)(2.2)\zeta_Q\zeta^{-1/3}}{1+2.2\zeta^{2/3}} \quad \text{for } \zeta \ge 0. \tag{5.15c}$$

In another publication,[57] I interpreted the meaning of sensitivity coefficients defined as in Eq. (5.9). In brief, if the sensitivity coefficient S is large (positive or negative), it magnifies the relative uncertainty in the measurement and shows that the C_n^2 estimate has a large uncertainty. If S is near zero, on the other hand, the predicted quantity is virtually independent of the measured quantity. I therefore concluded that the optimum value of S is near 1 or -1.

Figure 3 shows the sensitivity coefficients S_z and S_{u*} as functions of stability. From Eqs. (5.12) and (5.13) it is evident that these are both independent of the electromagnetic wavelength, and Figure 3 shows that neither is ever large enough to cause problems in estimating C_n^2. Note

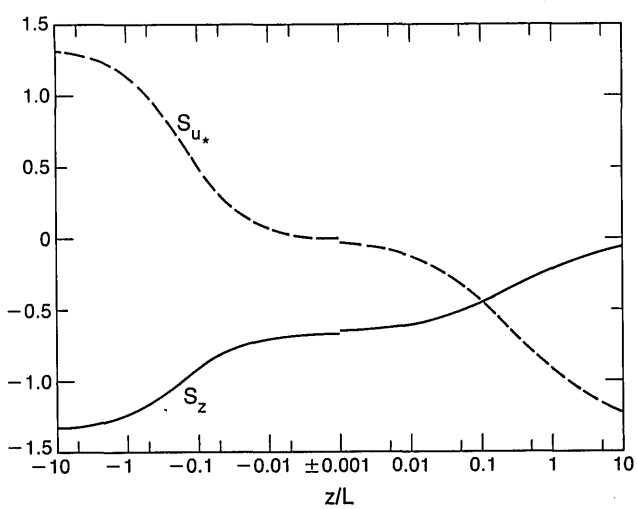

Fig. 3. The sensitivity coefficients S_z and S_{u_*} computed from Eqs. (5.12) and (5.13), respectively.

that, in the figure, S_{u*} is near zero for z/L near zero, as it must be, since $g(\zeta)$ becomes independent of ζ and thus of u_* near zero. The plot of S_z makes an interesting point. At large $-\zeta$, S_z approaches $-4/3$; near $\zeta = 0$, S_z is near $-2/3$; and at large ζ, S_z approaches 0. From Eqs. (5.1) and (4.19) we see that these sensitivity values are precisely the exponents of the z dependence of C_n^2 at these limits. Thus, if X is an independent variable and Y is a dependent variable, the sensitivity coefficient S relates them by $Y \propto X^S$ for small changes in X. This is true not only of S_z but of all the sensitivity coefficients that I will discuss.

Equations (5.14) and (5.15) show that S_{t*} and S_{q*} are much more complex than S_z and S_{u*}; S_{t*} and S_{q*} depend not only on the stability but also on the Bowen ratio and the electromagnetic wavelength (through A and B). Figures 4–7 show S_{t*} and S_{q*} for four electromagnetic wavelengths typical of the visible and near-infrared region (0.55 μm), the infrared window (10.6 μm), the near-millimeter region (337 μm = 890 GHz), and the radio region. The curves at the three stabilities shown in each figure, $\zeta = -1$, 0, 1, give a nearly inclusive envelope for the range of the sensitivity coefficients.

The strong dependence of the coefficients on the Bowen ratio in Figs. 4–7 is startling. In Eqs. (5.14b), (5.14c), (5.15b), and (5.15c), the sensitivity coefficients at neutral stability ($\zeta = 0$) are given by the first term on the right-hand side of each equation. Thus, at neutral stability, each coefficient has a simple pole at $\mathrm{Bo} = -B/KA$. Here each sensitivity coefficient becomes infinite, and it is impossible to estimate C_n^2 accurately. The second term on the right-hand side of each equation contains the stability dependence. Each of these terms has a simple pole at $\mathrm{Bo} = -0.61\overline{T}/[K(\rho + 0.61\overline{Q})]$ because of Eqs. (5.10) and (5.11). Here, too, it is impossible to estimate C_N^2. Clearly, from Figs. 4–7, the stability does not have a large effect on the sensitivity coefficients. The neutral-stability contribution sets the trend and the general level of the coefficients. Introducing the stability dependence does, however, produce a second pole in each coefficient.

The locations of the poles may not be detrimental for estimating C_n^2 over snow or sea ice at visible and infrared wavelengths. Figures 4 and 5 show that the poles have the greatest influence for Bowen ratios between -0.02 and -0.06. In my review I found few measurements that yielded Bowen ratios in this region. For near-millimeter and radio-wavelength estimates of C_n^2 (Figs. 6 and 7), however, the poles show large effects for Bowen ratios between 2 and 4, Bowen ratios that are commonly encountered over sea ice.

It is worthwhile to demonstrate the use of the sensitivity coefficients shown in Figs. 3–7. Suppose that we have measurements of z, u_*, t_*, and q_* and want to estimate C_n^2 for both visible and near-millimeter wavelengths. Assume that the relative uncertainty in z is ±2% (i.e., $dz/z = \pm 0.02$) and that the relative uncertainties in the flux quantities u_*, t_*, and q_* are typical of what is possible with an eddy correlation measurement of these [see Eqs. (4.1)–(4.3)], $du_*/u_* = \pm 0.1$ and $dt_*/t_* = dq_*/q_* = \pm 0.2$. Equation (5.5) yields the C_n^2 estimates, but we want to know the uncertainty in those estimates. That uncertainty can be computed from Eq. (5.9). Suppose that the u_*, t_*, and q_* values yield $\mathrm{Bo} \approx -1$ and $z/L \approx -0.1$. From Fig. 3 we therefore obtain $S_z = 0.9$ and $S_{u*} = 0.5$. For C_n^2 in the visible region, Fig. 4 gives S_{t*}

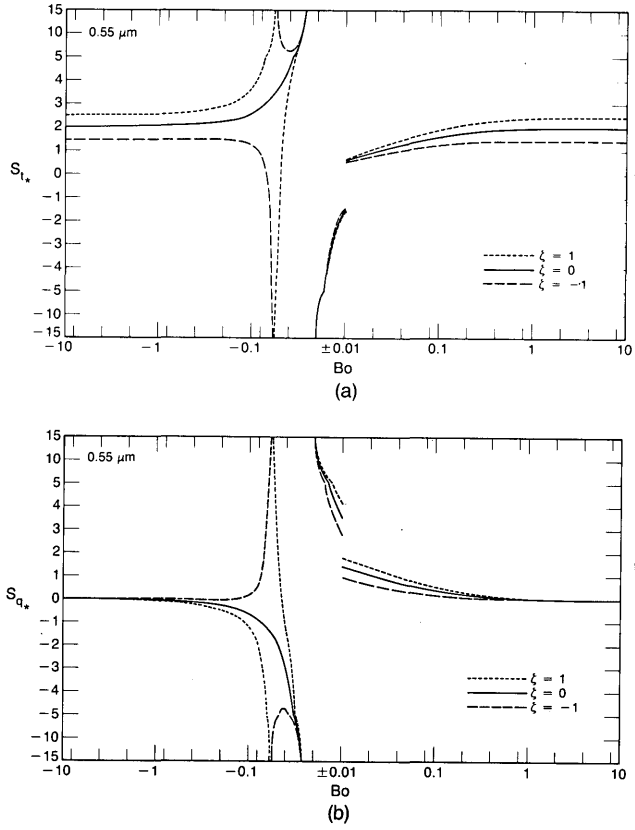

Fig. 4. The sensitivity coefficients (a) S_{t_*} and (b) S_{q_*} for an electromagnetic wavelength of 0.55 μm. The ambient conditions are P = 1000 hPa, $T = -10°C$, $Q = 1.93 \times 10^{-3}$ (i.e., a relative humidity of 90%). Notice that the ordinate changes scale at ±5.

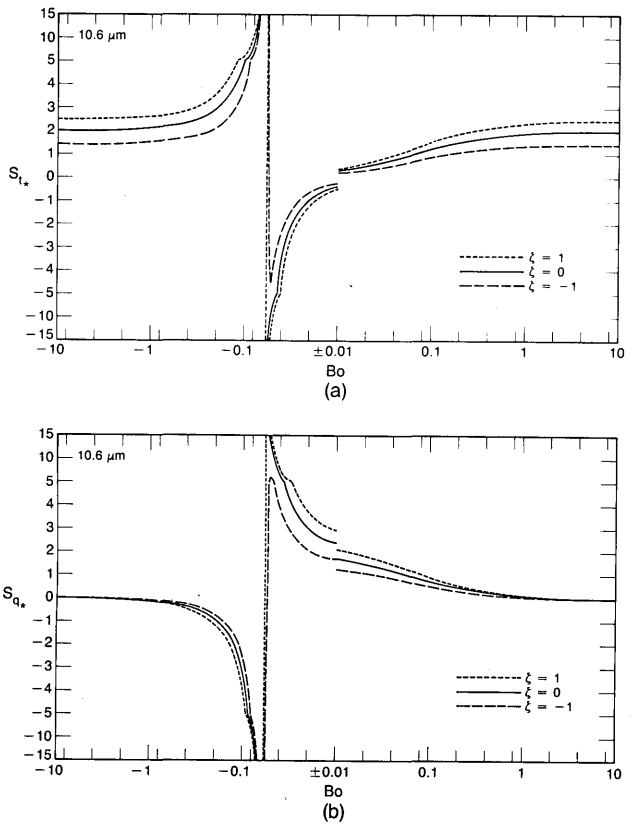

Fig. 5. As in Fig. 4 but for a wavelength of 10.6 μm.

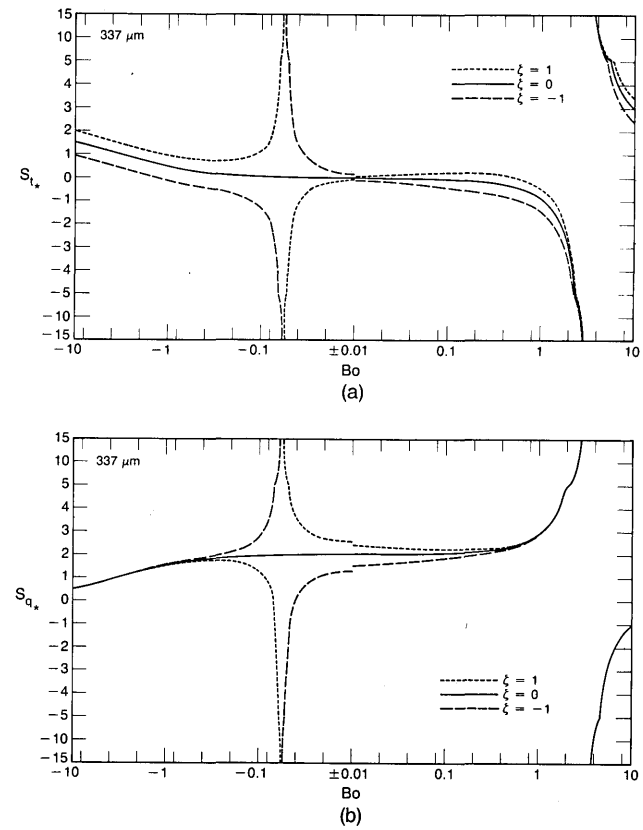

Fig. 6. As in Fig. 4 but for a wavelength of 337 μm (a frequency of 890 GHz).

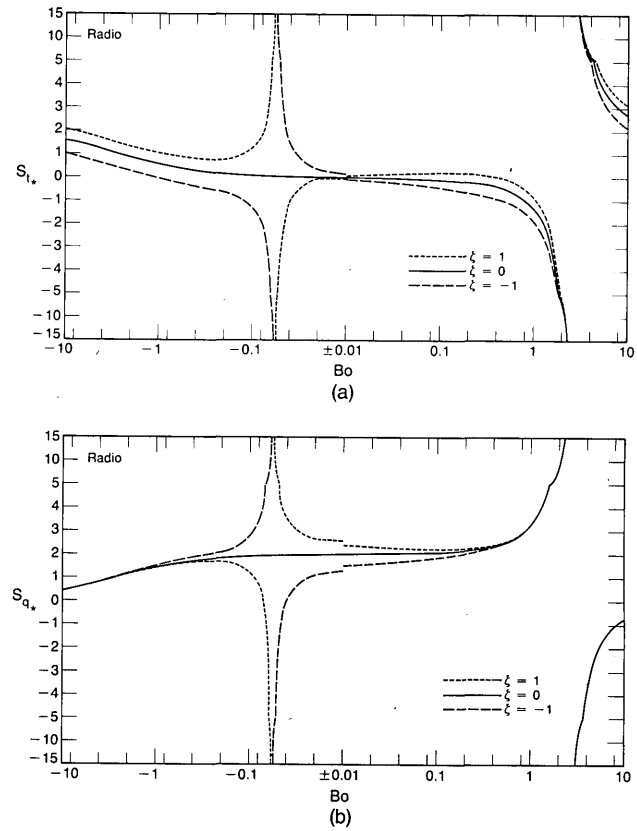

Fig. 7. As in Fig. 4 but for radio wavelengths.

≈ 2 and $S_{q*} = 0$. Hence, at 0.55 μm, $dC_n^2/C_n^2 = (\pm 2\%)(0.9) + (\pm 10\%)(0.5) + (\pm 20\%)(2) + (\pm 20\%)(0) = \pm 47\%$, the uncertainty in the C_n^2 estimate. For C_n^2 at 337 μm, Fig. 6 gives $S_{t*} \approx 0.5$ and $S_{q*} \approx 1.5$. Thus $(\pm 2\%)(0.9) + (\pm 10\%)(0.5) + (\pm 20\%)(0.5) + (\pm 20\%)(1.5) = \pm 47\%$ is also the uncertainty in this C_n^2 estimate. Clearly, our inability to measure the turbulent fluxes with precision leads to a fairly large uncertainty in the C_n^2 estimate.

6. ESTIMATING C_n^2 FROM ROUTINE METEOROLOGICAL OBSERVATIONS

Measuring the eddy correlations $\overline{uw}$, $\overline{wt}$, and $\overline{wq}$ and thereby obtaining u_*, t_*, and q_* is not easy. Measuring velocity, temperature, and humidity spectra in the inertial and inertial-convective subranges and then obtaining u_*, t_*, and q_* through the inertial-dissipation method[58] is somewhat easier but still requires sophisticated, fast-responding sensors. The way to obtain u_*, t_*, and q_* that is instrumentally and computationaly simplest is to measure the average wind speed, temperature, and absolute humidity at a reference height h (U_h, T_h, and Q_h, respectively) and the surface temperature and humidity, T_s and Q_s, and then to solve Eqs. (4.11)–(4.13) iteratively for u_*, t_*, q_*, and L.[56] That method of obtaining u_*, t_*, and q_* and the effects of uncertainties in the measured quantities, U_h, $\Delta T = T_s - T_h$, and $\Delta Q = Q_s - Q_h$, on the C_n^2 estimate are the subjects of this section.

Equations (4.4) and (4.11)–(4.17) contain the method of estimating u_*, t_*, and q_* from U_h, ΔT, and ΔQ. The solution is iterative. We first assume neutral stability ($h/L = 0$) and then compute initial estimates of u_*, t_*, q_*. With these, we compute L, ψ_m, and ψ_h; we then refit the data to compute new values of u_*, t_*, and q_*. We continue until the values converge, which usually takes fewer than five iterations. With these values of u_*, t_*, q_*, and L, it is simple to find C_n^2 at an arbitrary height and wavelength from Eq. (5.5).

On inspecting Eqs. (4.11)–(4.13), it is clear that we also need to know z_0, z_T, and z_Q to make the above computations. The roughness length z_0 has a one-to-one relationship with the drag coefficient at neutral stability at a reference height h:

$$C_{DNh} = [\kappa/\ln(h/z_0)]^{-2}. \tag{6.1}$$

Banke *et al.*[59] found that over snow-covered sea ice the neutral-stability drag coefficient at 10 m can be parameterized as

$$10^3 C_{DN10} = 1.10 + 0.072\xi, \tag{6.2}$$

where ξ is the root-mean-square (rms) surface roughness in centimeters found through a leveling survey. ξ is usually between 1 and 12 cm. Shirasawa[60] reported a similar increase in the drag coefficient with the roughness of the sea ice but was not as successful as Banke *et al.* in parameterizing it. Kondo and Yamazawa[61] likewise reported that the drag coefficient over a flat, snow-covered field increased with increasing roughness of the snow surface. I therefore hypothesized that Eq. (6.2) is an adequate model for both snow-covered sea ice and snow-covered ground.[62] On measuring, specifying, or guessing ξ, we can thus combine Eqs. (6.1) and (6.2) to find z_0.

I also developed a theoretical model to estimate z_T/z_0 and z_Q/z_0 from the roughness Reynolds number

Table 2. Values of the Coefficients in the Polynomials [Eq. (6.4)] That Predict z_s/z_0 for Temperature (i.e., z_T/z_0) and Water Vapor (i.e., z_Q/z_0)

Coefficient	$R_* \le 0.135$	$0.135 < R_* < 2.5$	$2.5 \le R_* \le 1000$
Temperature			
b_0	1.250	0.149	0.317
b_1	—	−0.550	−0.565
b_2	—	—	−0.183
Water Vapor			
b_0	1.610	0.351	0.396
b_1	—	−0.628	−0.512
b_2	—	—	−0.180

$$R_* = u_* z_0/\nu, \tag{6.3}$$

where ν is the kinetic viscosity of air.[62] Polynomials fitted to the model results have the form

$$\ln(z_s/z_0) = b_0 + b_1 \ln R_* + b_2(\ln R_*)^2, \tag{6.4}$$

where z_s is either z_T or z_Q. Table 2 gives the coefficients b_0, b_1, and b_2.

As in Section 5, the next question is, How does the uncertainty in the C_n^2 estimate depend on the uncertainties in the measured quantities z, U_h, ΔT, and ΔQ?

The answer to this question is derived from Eqs. (4.11)–(4.13) and from Eq. (5.8). To simplify the sensitivity analysis, I assume that the height z at which the C_n^2 estimate is desired is also the reference height h; that is, $z = h$ and $\zeta = h/L$. From Eqs. (4.11)–(4.13) and (6.1),

$$u_* = \frac{U_h}{C_{DNh}^{-1/2} - \kappa^{-1}\psi_m(\zeta)}, \tag{6.5}$$

$$t_* = \frac{-\Delta T}{C_{DNh}^{-1/2} - \kappa^{-1}[\ln(z_T/z_0) + \psi_h(\zeta)]}, \tag{6.6}$$

$$q_* = \frac{-\Delta Q}{C_{DNh}^{-1/2} - \kappa^{-1}[\ln(z_Q/z_0) + \psi_h(\zeta)]}. \tag{6.7}$$

In the sensitivity equation [Eq. (5.8)], we require du_*/u_*, dt_*/t_*, and dq_*/dq_*, which, from the above equations, are

$$\frac{du_*}{u_*} = \frac{dU_h}{U_h} + \frac{\zeta(\partial\psi_m/\partial\zeta)}{\kappa C_{DNh}^{-1/2} - \psi_m}\frac{d\zeta}{\zeta}, \tag{6.8}$$

$$\frac{dt_*}{t_*} = \frac{d\Delta T}{\Delta T} + \frac{\zeta(\partial\psi_h/\partial\zeta)}{\kappa C_{DNh}^{-1/2} - \ln(z_T/z_0) - \psi_h}\frac{d\zeta}{\zeta}, \tag{6.9}$$

$$\frac{dq_*}{q_*} = \frac{d\Delta Q}{\Delta Q} + \frac{\zeta(\partial\psi_h/\partial\zeta)}{\kappa C_{DNh}^{-1/2} - \ln(z_Q/z_0) - \psi_h}\frac{\partial\zeta}{\zeta}. \tag{6.10}$$

A complication here is that $d\zeta/\zeta$ depends on u_*, t_*, and q_*, which, in turn, depend on the measured quantities U_h, ΔT, and ΔQ. To get around this, we substitute Eqs. (6.8)–(6.10) into Eq. (5.7) and solve for $d\zeta/\zeta$. The result is

$$\frac{\partial\zeta}{\zeta} = D^{-1}\left(\frac{dz}{z} - 2\frac{dU_h}{U_h} + \frac{\zeta_T}{\zeta}\frac{d\Delta T}{\Delta T} + \frac{\zeta_Q}{\zeta}\frac{d\Delta Q}{\Delta Q}\right), \tag{6.11}$$

where

$$D = 1 + \frac{2\zeta(\partial\psi_m/\partial\zeta)}{\kappa C_{DNh}{}^{-1/2} - \psi_m} - \frac{\zeta(\partial\psi_h/\partial\zeta)}{\kappa C_{DNh}{}^{-1/2} - \ln(z_T/z_0) - \psi_h}. \tag{6.12}$$

Here I have ignored the small difference between z_T and z_Q and used z_T for both.

The next step is evluating $\partial\psi_m/\partial\zeta$ and $\partial\psi_h/\partial\zeta$. The ψ functions, defined by Eqs. (4.14)–(4.17), and the corresponding ϕ functions, Eqs. (4.8)–(4.10), are related by[41]

$$\psi(\zeta) = \int_0^\zeta \frac{1 - \phi(\zeta')}{\zeta'} d\zeta'. \tag{6.13}$$

Therefore, by Leibnitz's rule,

$$\frac{\partial\psi}{\partial\zeta} = \frac{1 - \phi(\zeta)}{\zeta}. \tag{6.14}$$

Using this result in Eq. (6.12) yields

$$D = 1 + \frac{2[1 - \phi_m(\zeta)]}{\kappa C_{DNh}{}^{-1/2} - \psi_m(\zeta)} - \frac{1 - \phi_h(\zeta)}{\kappa C_{DNh}{}^{-1/2} - \ln(z_T/z_0) - \psi_h(\zeta)}. \tag{6.15}$$

Finally, substituting Eqs. (6.11) and (6.14) into each of Eqs. (6.8)–(6.10) and substituting the resulting three equations into Eq. (5.8) gives a sensitivity equation for $C_n{}^2$ that depends on the measurements z, U_h, ΔT, and ΔQ:

$$\frac{dC_n{}^2}{C_n{}^2} = S_{zz}\frac{dz}{z} + S_U\frac{dU_h}{U_h} + S_{\Delta T}\frac{d\Delta T}{\Delta T} + S_{\Delta Q}\frac{d\Delta Q}{\Delta Q}. \tag{6.16}$$

On defining

$$F = D^{-1}\left\{\frac{[1 - \phi_m(\zeta)]\,S_{u_*}}{\kappa C_{DNh}{}^{-1/2} - \psi_m(\zeta)} + \frac{[1 - \phi_h(\zeta)][2 - \tfrac{1}{2}S_{u_*}]}{\kappa C_{DNh}{}^{-1/2} - \ln(z_T/z_0) - \psi_h(\zeta)}\right\}, \tag{6.17}$$

we see that these new sensitivity coefficients are related to the sensitivity coefficients found in Section 5:

$$S_{zz} = S_z + F, \tag{6.18}$$

$$S_U = S_{u_*} - 2F, \tag{6.19}$$

$$S_{\Delta T} = S_{t_*} + (\zeta_T/\zeta)F, \tag{6.20}$$

$$S_{\Delta Q} = S_{q_*} + (\zeta_Q/\zeta)F. \tag{6.21}$$

Figures 8–12 show plots of these sensitivity coefficients. The F term in each of the above equations is a function of the stability parameter ζ. At $\zeta = 0$, F is zero, since $\phi_m(0) = \phi_h(0) = 1$. Therefore, at neutral stability, the sensitivity coefficients of the routine meteorological measurements are the same as the flux-based sensitivity coefficients. Consequently, the $\zeta = 0$ lines in Figs. 9–12 are the same as the $\zeta = 0$ lines in Figs. 4–7.

Computing S_{zz}, S_U, $S_{\Delta T}$, and $S_{\Delta Q}$ requires specifying C_{DNh}. In my computations I assumed a reference height of 10 m and used C_{DN10} values of 1.172×10^{-3} and 1.964×10^{-3}; from Eq. (6.2) these correspond to rms surface roughnesses (ξ) of 1 and 12 cm, respectively. The sensitivity coefficients, however, depended only weakly on these C_{DN10} values, even over this maximum range of realistic values. Thus the figures show only the $C_{DN10} = 1.172 \times 10^{-3}$ case.

The sensitivity coefficients also depend implicitly on U_{10}, because to specify z_T/z_0 I had to estimate R_* from Eq. (6.3).

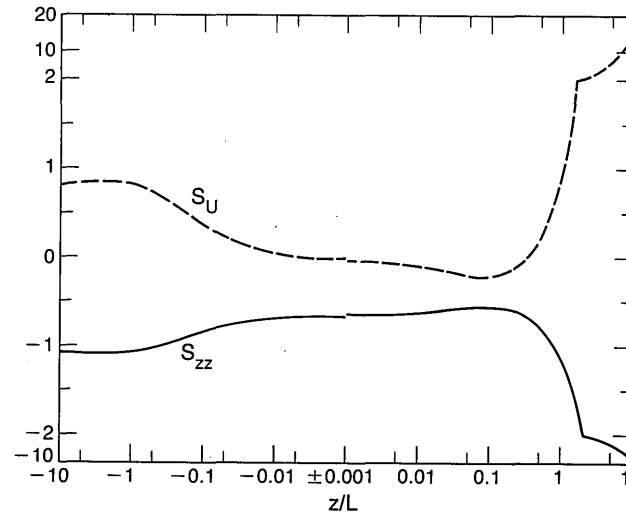

Fig. 8. The sensitivity coefficients S_{zz} and S_U computed from Eqs. (6.18) and (6.19). The reference height is 10 m, the wind speed there is 5 m sec^{-1}, and the neutral-stability drag coefficient referenced to 10 m is 1.172×10^{-3} (i.e., ξ = 1 cm). Notice that the ordinate changes scale at ±2.

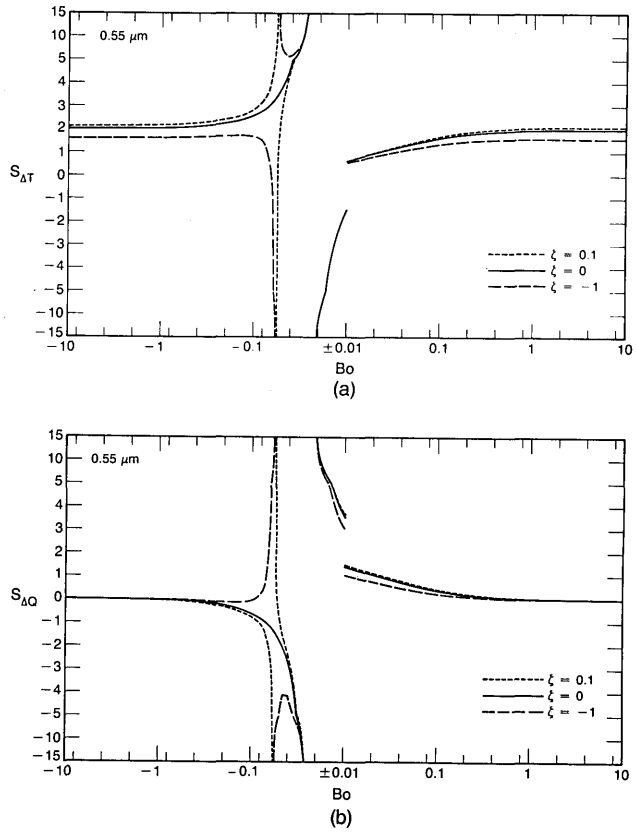

Fig. 9. The sensitivity coefficients (a) $S_{\Delta T}$ and (b) $S_{\Delta Q}$ for an electromagnetic wavelength of 0.55 μm. The reference height is 10 m, and the 10-m neutral-stability drag coefficient is $C_{DN10} = 1.172 \times 10^{-3}$ (i.e., ξ = 1 cm). The ambient conditions are P = 1000 hPa, $T = -10°C$, $Q = 1.93 \times 10^{-3}$ kg m^{-3} (i.e., relative humidity of 90%), and U = 5 m sec^{-1}. Notice that the ordinate changes scale at ±5.

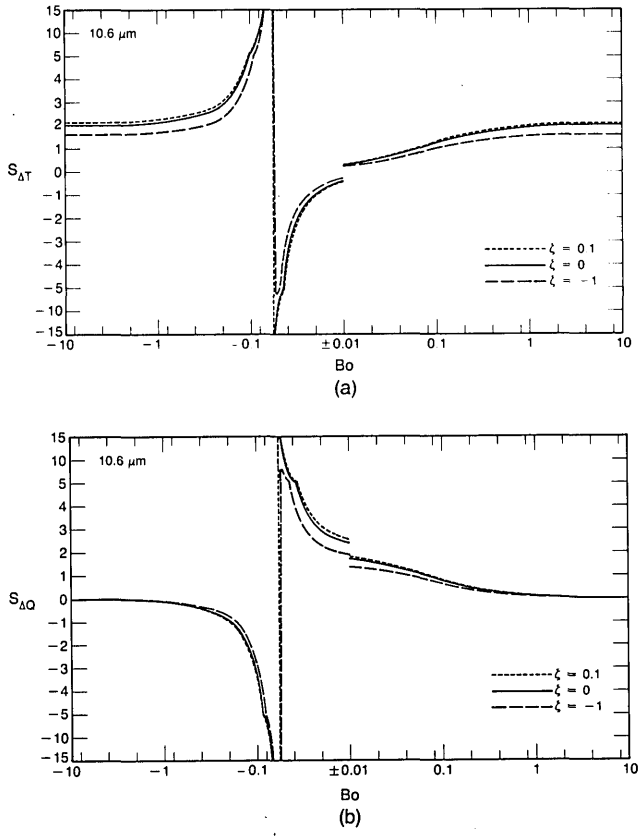

Fig. 10. As in Fig. 9 but for a wavelength of 10.6 μm.

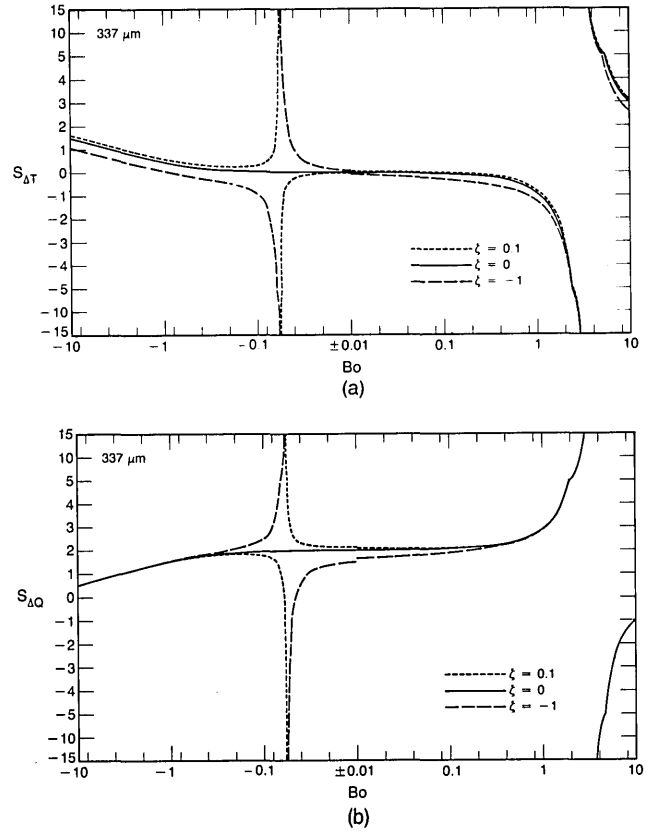

Fig. 11. As in Fig. 9 but for a wavelength of 337 μm (a frequency of 890 GHz).

Specifying C_{DN10} or ξ gives z_0 from Eqs. (6.1) and (6.2). To find u_* I chose a U_{10} value and used this z_0 value in Eq. (4.11), assuming neutral stability. Again, S_{zz}, S_U, $S_{\Delta T}$, and $S_{\Delta Q}$ depend so weakly on U_{10} that I chose a typical midrange value, $U_{10} = 5$ m sec^{-1}, in preparing Figs. 8–12.

The sensitivity coefficients S_z, S_{u*}, S_{zz}, and S_U do not depend on ambient temperature and humidity. The coefficients S_{t*}, S_{q*}, $S_{\Delta T}$, and $S_{\Delta Q}$ have such a weak dependence on temperature and humidity that Figs. 5–8 and 9–12, which are based on $T = -10$°C and $Q = 1.93 \times 10^{-3}$ kg m^{-3} (relative humidity of 90%), represent most realistic conditions over snow and sea ice.

According to Fig. 8, S_{zz} and S_U are reasonably well behaved for most stabilities. As with S_{u*}, S_U approaches 0 at neutral stability, since the main impact of wind speed on an estimate of C_n^2 is through the stability parameter z/L. For $z/L > 1$, the magnitudes of both S_U and S_{zz} begin increasing. Consequently, in this region, uncertainties in U_h or h could be detrimental to the C_n^2 estimates. Fortunately, z/L values of >2 are rare in the surface layer.

The three lines ($\zeta = -1$, 0, 0.1) in Figs. 9–12 more or less bracket the range of the sensitivity coefficients. As with the S_{t*} and S_{q*} values, $S_{\Delta T}$ and $S_{\Delta q}$ each have a simple pole at Bo $= -B/KA$ for neutral stability. When we introduce stability effects, both also have a simple pole at Bo $= -0.61\overline{T}/[K(\rho + 0.61\overline{Q})]$. It is therefore impossible to estimate C_n^2 accurately if the Bowen ratio is in the vicinity of the poles. We can easily identify problematic data, since the Bowen ratio is derived directly from the measured quantities by using Eqs. (4.12), (4.13), and (5.3), assuming that $z_T \approx z_Q$:

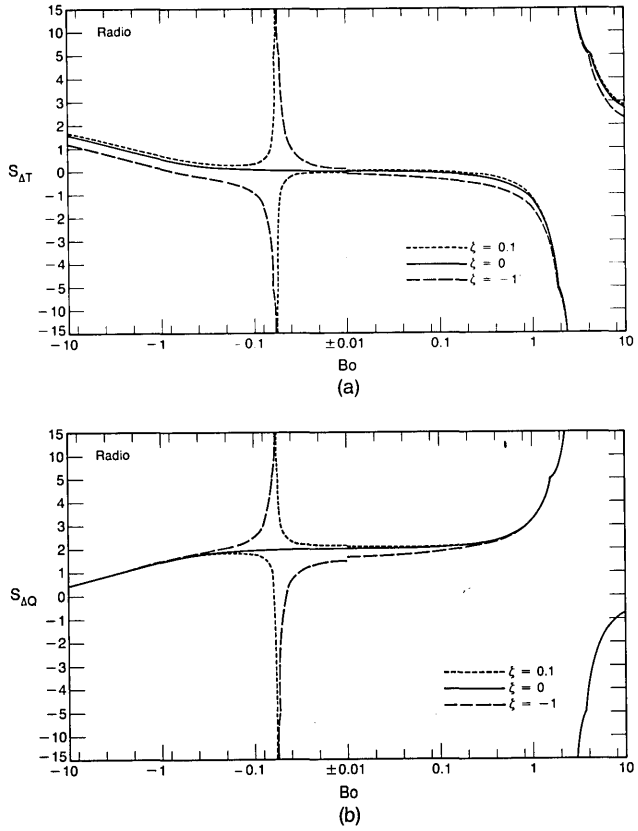

Fig. 12. As in Fig. 9 but for radio wavelengths.

$$\mathrm{Bo} = \frac{\Delta T}{K \Delta Q} . \tag{6.22}$$

Despite the similarity of the values of S_{t_*} and $S_{\Delta T}$ and of S_{q_*} and $S_{\Delta Q}$, estimates of C_n^2 based on U_h, ΔT, and ΔQ are likely to be more uncertain than estimates based on u_*, t_*, and q_*. This is because the relative uncertainties in ΔT and ΔQ may well be larger than for t_* and q_*. Measuring the temperature and the absolute humidity of the snow surface is difficult because the measuring device often ruins the integrity of the surface or otherwise disturbs its thermal regime[63]; uncertainties in T_s and Q_s can therefore be large. The small vertical temperature and humidity gradients that usually exist over snow, especially over snow-covered sea ice, exacerbate this problem. With small gradients, it would not be unusual to have uncertainties in ΔT and ΔQ that are nearly as large as their absolute values. I have developed a noninvasive method of measuring the snow-surface temperature that may minimize the uncertainty in this measurement,[63] but more research is necessary to ensure accurate T_s and Q_s measurements.

7. DISCUSSION

The methods that I have described for estimating C_n^2 have two primary uses. The first is for comparing values of C_n^2 obtained directly from electro-optical instruments with values estimated from micrometeorological measurements, with the objective of verifying elements of the theory contained in Sections 4–6. The basic question here is, Can point measurements be used to predict path-averaged quantities? Davidson *et al.*[14] used the methods that I have described, with minor variations, to make such a comparison with data collected over the ocean. Although the agreement between their electro-optical and meteorological estimates of C_n^2 was encouraging, the data scatter was rather large. Evidently, Davidson *et al.* did not realize that the accuracy of their meteorologically derived C_n^2 estimates depended on the Bowen ratio, because they did not mention the range of Bowen ratios encountered, nor did they provide enough information for me to estimate Bowen ratios. Although it is unlikely that the scatter in their optical C_n^2 values was due to the Bowen ratio, since Bo is usually positive over the ocean (see Figs. 4 and 9), I encourage experimentalists to consider this source of uncertainty in future comparisons.

The second, probably broader, use of these methods for estimating C_n^2 is predicting C_n^2 from routine meteorological observations.[8,64] On the basis of such estimates we could then prepare C_n^2 climatologies for various locales and for various meteorological conditions[8] for the purpose of evaluating how electro-optical sensors would function in such conditions. Again, though, if the Bowen ratio indicated by the meteorological data [i.e., Eq. (5.3) or Eq. (6.22)] is near one of the poles in Figs. 4–7 or 9–12, the uncertainty of the associated C_n^2 estimate may be prohibitively large.

Although I have concentrated on estimating C_n^2 over snow and sea ice, there is nothing to preclude using my methods over other horizontally homogeneous surfaces. In fact, the development in Section 5 on estimating C_n^2 from turbulent fluxes applies to any surface. Only the sensitivity coefficients, which were computed for $T = -10°\mathrm{C}$ and $Q = 1.93 \times 10^{-3}$, specify the nature of the surface. In estimating C_n^2 from routine meteorological observations (Section 6), the only changes that are necessary for using my method over other surfaces would be in estimating z_0 (or C_{DNh}), z_T, and z_Q. The equations that I give for these are valid only over snow and snow-covered sea ice. Models for z_0, z_T, and z_Q do, however, exist for other surfaces. Liu *et al.*,[65] for example, developed a model for z_s/z_0 over the ocean and used Kondo's[66] parameterization of the 10-m drag coefficient to find z_0. Brutsaert[67] formulated a model for z_s/z_0 over an arbitrary solid surface, and Garratt and Hicks[68] formulated another model for a variety of surfaces; for z_0 here one could consult Garratt's[69] review of drag coefficients measured over various geophysical surfaces.

In estimating C_n^2 from routine meteorological observations, I chose to base estimates on the temperature and humidity differences between the reference height h and the surface. It is, however, also possible to base C_n^2 estimates on the temperature and humidity differences betweent the two heights h and h', where h' is above the surface and $h > h'$. A sensitivity analysis of this estimation procedure and some physical insight would show why my original method is better. C_n^2 would now also suffer from the additional uncertainty in the measurement of h'. More importantly, though, the relative uncertainties in the measured quantities $\Delta T' = T_{h'} - T_h$ and $\Delta Q' = Q_{h'} - Q_h$ would probably be larger than for $\Delta T = T_s - T_h$ and $\Delta Q = Q_s - Q_h$, since the largest temperature and humidity gradients are in the immediate vicinity of the surface. Thus, although the sensitivity coefficients $S_{\Delta T'}$ and $S_{\Delta Q'}$ would probably be smaller than $S_{\Delta T}$ and $S_{\Delta Q}$, the larger relative uncertainties, $\mathrm{d}\Delta T'/\Delta T'$ and $\mathrm{d}\Delta Q'/\Delta Q'$, would certainly nullify this benefit.

8. CONCLUSIONS

The fundamental equation on which most of my analysis rests is Eq. (5.1):

$$C_n^2 = z^{-2/3} n_*^2 g(\zeta), \tag{8.1}$$

with $g(\zeta)$ given by Eqs. (4.19). Although the validity of this equation has been checked experimentally only indirectly and only at visible wavelengths, much associated experimental and theoretical work argues in support of its accuracy. One use for the methods of estimating C_n^2 that I have discussed could therefore be finally to test Eq. (8.1) directly and to do a careful analysis of the experimental uncertainties.

The derivation of a means of estimating these uncertainties is one of the main results of this paper. Estimating C_n^2 from the flux scales u_*, t_*, and q_* requires only four equations, Eqs. (5.5), (4.19a), (4.19b), and (4.4). Estimating C_n^2 from the routine meteorological data U_h, ΔT, and ΔQ requires only a few additional equations, namely, Eqs. (6.5)–(6.7) and some others. However, evaluating the uncertainty in either estimate of C_n^2 is much more difficult because of the nonlinear dependence of C_n^2 on the measured quantities. My analysis shows that the sensitivity coefficients that predict the uncertainty in C_n^2 are generally strong functions of the Bowen ratio Bo. In nonneutral stability conditions, S_{t_*}, S_{q_*}, $S_{\Delta T}$, and $S_{\Delta Q}$ each become infinite at two values of Bo in the interval $[-10, 10]$. In the vicinity of these singularities it is impossible to estimate C_n^2 accurately. My plots of the sensitivity coefficients S_{t_*}, S_{q_*}, $S_{\Delta T}$, and $S_{\Delta Q}$ (Figs. 4–7 and 9–12) are thus important warnings to anyone who would try

to estimate C_n^2 with arbitrary accuracy at an arbitrary Bowen ratio.

A second major result of this paper is my derivation of analytic expressions in four useful wavelength regions for the functions $A(\lambda, P, T, Q)$ and $B(\lambda, P, T, Q)$ that appear in Eq. (2.9). Equations already existed for the visible (to near-infrared) region (0.36–3 μm) and for radio wavelengths (>3 mm). I added equations for an infrared window (7.8–19 μm) and for near-millimeter wavelengths (0.3–3 mm) and then computed the sensitivity coefficients in each of the four wavelength regions where scintillation and, consequently, C_n^2 are commonly measured.

ACKNOWLEDGMENTS

I would like to thank R. J. Hill for helpful discussions, E. E. Gossard for reviewing the manuscript, two anonymous reviewers for useful suggestions, and the U.S. National Research Council for supporting me as a NOAA/WPL Research Associate.

*Present address, U.S. Army Cold Regions Research and Engineering Laboratory, Hanover, New Hampshire 03755-1290.

REFERENCES

1. R. S. Lawrence and J. W. Strohbehn, "A survey of clear-air propagation effects relevant to optical communications," Proc. IEEE **58,** 1523–1545 (1970).
2. R. J. Hill and S. F. Clifford, "Modified spectrum of atmospheric temperature fluctuations and its application to optical propagation," J. Opt. Soc. Am. **68,** 892–899 (1978).
3. S. F. Clifford, G. R. Ochs, and R. S. Lawrence, "Saturation of optical scintillation by strong turbulence," J. Opt. Soc. Am. **64,** 148–154 (1974).
4. T.-I. Wang, G. R. Ochs, and S. F. Clifford, "A saturation-resistant optical scintillometer to measure C_n^2," J. Opt. Soc. Am. **68,** 334–338 (1978).
5. R. J. Hill, "Theory of measuring the path-averaged inner scale of turbulence by spatial filtering of optical scintillation," Appl. Opt. **21,** 1201–1211 (1982).
6. R. S. Lawrence, G. R. Ochs, and S. F. Clifford, "Measurement of atmospheric turbulence relevant to optical propagation," J. Opt. Soc. Am. **60,** 826–830 (1970).
7. M. A. Kallistratova and D. F. Timanovskiy, "The distribution of the structure constant of refractive index fluctuations in the atmospheric surface layer," Izv. Atmos. Oceanic Phys. **7,** 46–48 (1971).
8. M. L. Wesely and E. C. Alcarez, "Diurnal cycles of the refractive index structure function coefficient," J. Geophys. Res. **78,** 6224–6232 (1973).
9. E. L. Andreas, "Spectral measurements in a disturbed boundary layer over snow," J. Atmos. Sci. **44,** 1912–1939 (1987).
10. V. I. Tatarskii, *The Effects of the Turbulent Atmosphere on Wave Propagation* (Israel Program for Scientific Translations, Jerusalem, 1971); also publication TT 68-50464 (National Technical Information Service, Springfield, Va.).
11. C. A. Friehe, J. C. LaRue, F. H. Champagne, C. H. Gibson, and G. F. Dreyer, "Effects of temperature and humidity fluctuations on the optical refractive index in the marine boundary layer," J. Opt. Soc. Am. **65,** 1502–1511 (1975).
12. J. T. Priestley and R. J. Hill, "Measuring high-frequency humidity, temperature and radio refractive index in the surface layer," J. Atmos. Oceanic Technol. **2,** 233–251 (1985).
13. C. A. Friehe, "Estimation of the refractive-index temperature structure parameter over the ocean," Appl. Opt. **16,** 334–340 (1977).
14. K. L. Davidson, G. E. Schacher, C. W. Fairall, and A. K. Goroch, "Verification of the bulk method for calculating overwater optical turbulence," Appl. Opt. **20,** 2919–2924 (1981).
15. J. C. Wyngaard and M. A. Lemone, "Behavior of the refractive index structure parameter in the entraining convective boundary layer," J. Atmos. Sci. **37,** 1573–1585 (1980).
16. W. Kohsiek, "Measuring C_T^2, C_Q^2, and C_{TQ} in the unstable surface layer, and relations to the vertical fluxes of heat and moisture," Boundary-Layer Meteorol. **24,** 89–107 (1982).
17. E. E. Gossard, "Power spectra of temperature, humidity and refractive index from aircraft and tethered balloon measurements," IRE Trans. Antennas Propag. **AP-8,** 186–201 (1960).
18. M. L. Wesely, "The combined effect of temperature and humidity fluctuations on refractive index," J. Appl. Meteorol. **15,** 43–49 (1976).
19. R. J. Hill, S. F. Clifford, and R. S. Lawrence, "Refractive-index and absorption fluctuations in the infrared caused by temperature, humidity, and pressure fluctuations," J. Opt. Soc. Am. **70,** 1192–1205 (1980).
20. G. A. McBean and J. A. Elliott, "Pressure and humidity effects on optical refractive-index fluctuations," Boundary-Layer Meteorol. **20,** 101–109 (1981).
21. J. C. Owens, "Optical refractive index of air: dependence on pressure, temperature and composition," Appl. Opt. **6,** 51–59 (1967).
22. R. J. Hill and R. S. Lawrence, "Refractive index of water vapor in infrared windows," Infrared Phys. **26,** 371–376 (1986).
23. R. J. Hill, R. S. Lawrence, and J. T. Priestley, "Theoretical and calculational aspects of the radio refractive index of water vapor," Radio Sci. **17,** 1251–1257 (1982).
24. G. Boudouris, "On the index of refraction of air, the absorption and dispersion of centimeter waves by gases," J. Res. Natl. Bur. Stand. Sect. D **67,** 631–684 (1963).
25. B. R. Bean and E. J. Dutton, *Radio Meteorology*, Natl. Bur. Stand. (U.S.) Monogr. **92** (1966).
26. R. J. Hill, "Dispersion by atmospheric water vapor at frequencies less than 1 THz," IEEE Trans. Antennas Propag. (to be published).
27. R. A. Bohlander, R. W. McMillan, and J. J. Gallagher, "Atmospheric effects on near-millimeter-wave propagation," Proc. IEEE **73,** 49–60 (1985).
28. W. Kohsiek, "Optical and in situ measuring of structure parameters relevant to temperature and humidity, and their application to the measuring of sensible and latent heat flux," NOAA Tech. Memo. ERL WPL-96 (Wave Propagation Laboratory, Boulder, Colo., 1982).
29. R. W. McMillan, R. A. Bohlander, G. R. Ochs, R. J. Hill, and S. F. Clifford, "Millimeter wave atmospheric turbulence measurements: preliminary results and instrumentation for future measurements," Opt. Eng. **22,** 32–39 (1983).
30. A. M. Obukhov, "Turbulence in an atmosphere with a nonuniform temperature," Boundary-Layer Meteorol. **2,** 7–29 (1971).
31. N. E. Busch, "On the mechanics of atmospheric turbulence," in *Workshop on Micrometeorology*, D. A. Haugen, ed. (American Meteorological Society, Boston, Mass., 1973), pp. 1–65.
32. J. A. Businger, "Turbulent transfer in the atmospheric surface layer," in *Workshop on Micrometeorology*, D. A. Haugen, ed. (American Meteorological Society, Boston, Mass., 1973), pp. 67–100.
33. J. C. Wyngaard, "On surface-layer turbulence," in *Workshop on Micrometeorology*, D. A. Haugen, ed. (American Meteorological Society, Boston, Mass., 1973), pp. 101–149.
34. H. A. Panofsky and J. A Dutton, *Atmospheric Turbulence: Models and Methods for Engineering Applications* (Wiley-Interscience, New York, 1984).
35. J. A. Businger, J. C. Wyngaard, Y. Izumi, and E. F. Bradley, "Flux-profile relationships in the atmospheric surface layer," J. Atmos. Sci. **28,** 181–189 (1971).
36. A. J. Dyer, "A review of flux-profile relationships," Boundary-Layer Meteorol. **7,** 363–372 (1974).
37. A. M. Yaglom, "Comments on wind and temperature flux-profile relationships," Boundary-Layer Meteorol. **11,** 89–102 (1977).
38. A. J. Dyer and E. F. Bradley, "An alternative analysis of flux-

gradient relationships at the 1976 ITCE," Boundary-Layer Meteorol. **22,** 3–19 (1982).
39. W. G. Large and S. Pond, "Sensible and latent heat flux measurements over the ocean," J. Phys. Oceanogr. **12,** 464–482 (1982).
40. J. Wieringa, "A revaluation of the Kansas mast influence on measurements of stress and cup anemometer overspeeding," Boundary-Layer Meteorol. **18,** 411–430 (1980).
41. C. A. Paulson, "The mathematical representation of wind speed and temperature profiles in the unstable surface layer," J. Appl. Meteorol. **9,** 857–861 (1970).
42. J. C. Wyngaard, Y. Izumi, and S. A. Collins, Jr., "Behavior of the refractive-index-structure parameter near the ground," J. Opt. Soc. Am. **61,** 1646–1650 (1971).
43. C. W. Fairall, G. E. Schacher, and K. L. Davidson, "Measurements of the humidity structure function parameters, C_q^2 and C_{Tq}, over the ocean," Boundary-Layer Meteorol. **19,** 81–92 (1980).
44. E. L. Andreas, "On the Kolmogorov constants for the temperature-humidity cospectrum and the refractive index spectrum," J. Atmos. Sci. **44,** 2399–2406 (1987).
45. J. C. Wyngaard and O. R. Coté, "The budgets of turbulent kinetic energy and temperature variance in the atmospheric surface layer," J. Atmos. Sci. **28,** 190–201 (1971).
46. J. C. Kaimal, J. C. Wyngaard, Y. Izumi, and O. R Coté, "Spectral characteristics of surface-layer turbulence," Q. J. R. Meteorol. Soc. **98,** 563–589 (1972).
47. C. W. Fairall, R. Markson, G. E. Schacher, and K. L. Davidson, "An aircraft study of turbulence dissipation rate and temperature structure function in the unstable marine atmospheric boundary layer," Boundary-Layer Meteorol. **19,** 453–469 (1980).
48. G. E. Schacher, K. L. Davidson, T. Houlihan, and C. W. Fairall, "Measurements of the rate of dissipation of turbulent kinetic energy, ϵ, over the ocean," Boundary-Layer Meteorol. **20,** 321–330 (1981).
49. K. L. Davidson, T. M. Houlihan, C. W. Fairall, and G. E. Schacher, "Observation of the temperature structure function parameter, C_T^2, over the ocean," Boundary-Layer Meteorol. **15,** 507–523 (1978).
50. K. E. Kunkel, D. L. Walters, and G. A. Ely, "Behavior of the temperature structure parameter in a desert basin," J. Appl. Meteorol. **20,** 130–136 (1981).
51. J. C. Wyngaard, W. T. Pennell, D. H. Lenschow, and M. A. LeMone, "The temperature-humidity covariance budget in the convective boundary layer," J. Atmos. Sci. **35,** 47–58 (1978).
52. B. B. Hicks and H. C. Martin, "Atmospheric turbulent fluxes over snow," Boundary-Layer Meteorol. **2,** 496–502 (1972).
53. L. G. Yelagina, B. M. Korpov, and D. F. Timanovskiy, "Certain characteristics of the atmospheric surface layer above snow," Izv. Atmos. Oceanic Phys. **14,** 652–655 (1978).
54. D. C. McKay and G. W. Thurtell, "Measurements of the energy fluxes involved in the energy budget of a snow cover," J. Appl. Meteorol. **17,** 339–349 (1978).
55. M. R. Thorpe, E. G. Banke, and S. D. Smith, "Eddy correlation measurements of evaporation and sensible heat flux over Arctic sea ice," J. Geophys. Res. **78,** 3573–3584 (1973).
56. E. L. Andreas and A. P. Makshtas, "Energy exchange over Antarctic sea ice in the spring," J. Geophys. Res. **90,** 7199–7212 (1985).
57. E. L. Andreas, "Atmospheric stability from scintillation measurements," Appl. Opt. (to be published).
58. C. W. Fairall and S. E. Larson, "Inertial-dissipation methods and turbulent fluxes at the air-ocean interface," Boundary-Layer Meteorol. **34,** 287–301 (1986).
59. E. G. Banke, S. D. Smith, and R. J. Anderson, "Drag coefficients at AIDJEX from sonic anemometer measurements," in *Sea Ice Processes and Models,* R. S. Pritchard, ed. (U. Washington Press, Seattle, Wash., 1980), pp. 430–442.
60. K. Shirasawa, "Studies on wind stress on sea ice," Low Temp. Sci. A **40,** 101–118 (1981) (in Japanese; English summary).
61. J. Kondo and H. Yamazawa, "Bulk transfer coefficient over a snow surface," Boundary-Layer Meteorol. **34,** 123–135 (1986).
62. E. L. Andreas, "A theory for the scalar roughness and the scalar transfer coefficients over snow and sea ice," Boundary-Layer Meteorol. **38,** 159–184 (1987).
63. E. L. Andreas, "A new method of measuring the snow-surface temperature," Cold Regions Sci. Technol. **12,** 139–156 (1986).
64. K. E. Kunkel and D. L. Walters, "Modeling the diurnal dependence of the optical refractive index structure parameter," J. Geophys. Res. **88,** 10999–11004 (1983).
65. W. T. Liu, K. B. Katsaros, and J. A. Businger, "Bulk parameterization of air-sea exchanges of heat and water vapor including the molecular constraints at the interface," J. Atmos. Sci. **36,** 1722–1735 (1979).
66. J. Kondo, "Air-sea bulk transfer coefficients in diabatic conditions," Boundary-Layer Meteorol. **9,** 91–112 (1975).
67. W. Brutsaert, "The roughness length for water vapor, sensible heat, and other scalars," J. Atmos. Sci. **32,** 2028–2031 (1975).
68. J. R. Garratt and B. B. Hicks, "Momentum, heat and water vapour transfer to and from natural and artificial surfaces," Q. J. R. Meteorol. Soc. **99,** 680–687 (1973).
69. J. R. Garratt, "Review of drag coefficients over oceans and continents," Mon. Weather Rev. **105,** 915–929 (1977).